2011

DIANA

ELEMENTS

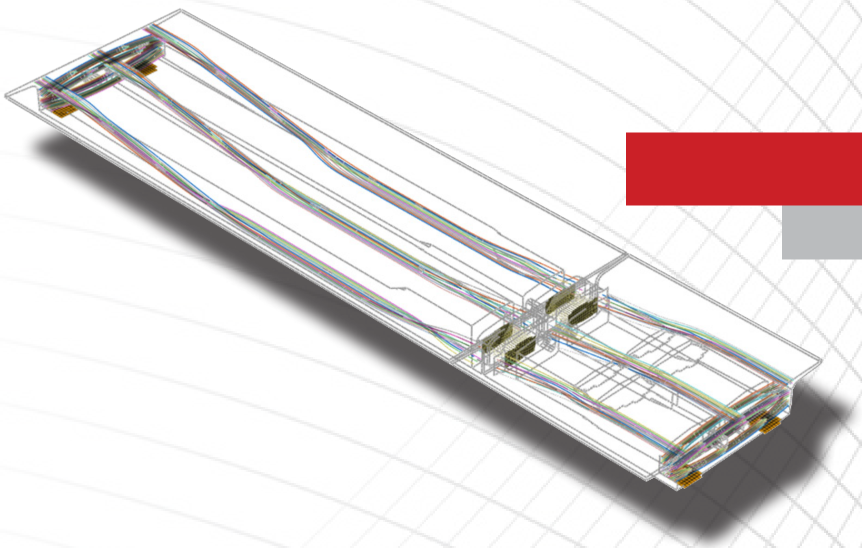

TNO DIANA
A TNO Company

Content

3 New Release: DIANA 9.4.4

11 Evaluation of the risk of Cracking in thin concrete walls due to hydration heat
C. ZANOTTI, G.PLIZZARI (UNIV. BRESCIA), A.MEDA (UNIV. ROME), S.CANGIANO (CTG ITALCEMENTI GROUP)

16 Prediction of Crack-width & Crack-pattern
G. SCHREPPERS, C. FRISSEN & H. KANG

25 London Conference
DAVID BEGG

26 Nonlinear Seismic Tunnel-Soil Interaction Analysis
PRANESH CHATTERJEE

28 Control of Cracking in RC Structures
C. DAMONI, B. BELLETTI (UNIV. PARMA) & G. LILLIU (TNO DIANA BV)

30 Staff & Events at TNO DIANA BV

Colophon
DIANA ELEMENTS *is published by*
TNO DIANA BV
Delftechpark 19a
2628 XJ Delft
The Netherlands

T +31 (0) 88 24262 00
F +31 (0) 88 34262 99
eFax +31 (0) 84 74990 28

info@tnodiana.com
http://tnodiana.com

DIANA ELEMENTS is distributed to TNO DIANA BV customers and other interested persons.

The editors welcome letters, technical articles, news of forthcoming events, publications of topical interest and project descriptions.

Editorial

There are only a few working days left until the end of the year. This is a good moment to look back to the very dynamic year 2011, and to take a preview to what we may expect from 2012.

I just want to give you a short overview of the most important activities at TNO DIANA in 2011:

- DIANA 9.4.3 release was presented
- New training courses for Geotechnical and Dam analysis were organised, in addition to the Reinforced Concrete course that was completely revised.
- The company website was completely restructured highlighting the different application areas of DIANA
- We attended nine conferences and participated, with success, in both Concrack and ICOLD benchmarks
- We have set up a range of web-seminars and online courses which were received very well.

We can look back to a year in which we have experienced, again, a strongly increasing interest in the market for full 3-dimensional non-linear analysis.

The models and analyses that DIANA users are performing grow in terms of number of elements. We are especially pleased that many of the DIANA users every time again adapt new aspects of the modelling and analysis capabilities of the software and doing so expand the application of DIANA in their organisations.

In January 2012 we will introduce DIANA 9.4.4, and in this issue you find an overview of the new functionalities of this new version. We will be present at several conferences and exhibitions and we have planned a series of webinars in which every month a new topic will be addressed. In April/May we plan to organise a seminar dedicated to earthquake analysis. Throughout the year our development team will work on the integration of pre-processing, post-processing and solver functionality. With this integration we will make the DIANA analysis power available for wider group of customers.

The TNO DIANA wishes you a good end of the year and best wishes for 2012.

Gerd-Jan Schreppers
Director TNO DIANA BV

DIANA - New Features in 9.4.4

This new DIANA version will be available in January 2012.

It will be available to download for all DIANA customers who have a web-account and will be distributed to DIANA customers who are entitled to get updates on request.

Among many other new functions, DIANA 9.4.4 offers new application modules for reinforcement design checks and stiffness adaptation analysis. These new modules will make it possible to optimise the design of structures and to assess the additional capacity in the design of reinforced concrete structures.

For the geotechnical engineer it is now possible to do a phi-C reduction analysis by using the new Strength reduction analysis application module. This new module will allow to calculate to shear-capacity in geotechnical structures.

At a Glance...

Elements

- Beam elements
- Curved shells with drilling rotations
- Bond-slip reinforcements in 2D and shell interface elements
- Boundary surface elements
- Fluid-structure interface elements
- Composed lines
- Pre-stressing and post-tensioning of embedded reinforcements

Material models

- Tension cut-off for Mohr-Coulomb and Drucker-Prager
- Engineering input for Modified Mohr-Coulomb
- Extensions for total strain crack model
- Solidification or evaporation
- D-min soil model
- Classic Brick model for soil
- Modified two-surface model for cyclic behavior of steel
- Menegotto-Pinto plasticity model for reinforcements
- Van Genuchten relative conductivity model for groundwater flow

Analysis Functionality

- User-supplied subroutines
- Linear constraints for flow analysis
- Prescribed accelerations
- Geometrical nonlinear analysis
- Arc-length control
- Logging
- Damping and inertia forces
- Euro-code 8 elastic and design spectra
- Transient dynamic analysis
- Spectral response analysis
- Strength reduction analysis
- Reinforcement grid design checking
- Stiffness adaptation analysis
- Crack-width results

Pre- and post-processing

iDIANA

- Importing external files
- CAD based reinforcements
- Labelling and coloring reinforcements
- Color and style of vector plots

FX+ for DIANA

- Distributed moment load
- Material properties
- Reinforcement sets
- Running DIANA
- Center or element and integration-point results
- Embedded reinforcement results

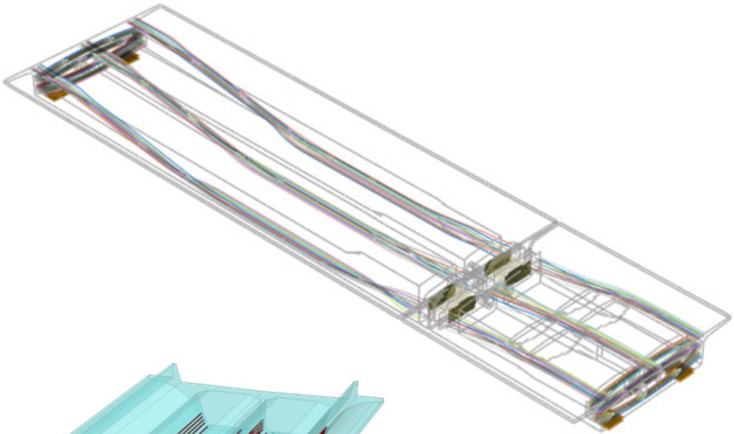

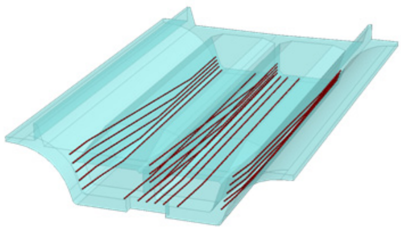

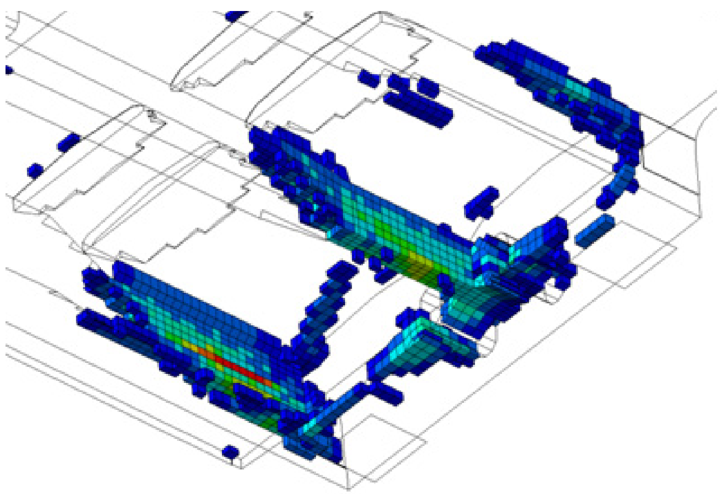

9.4.4. In more detail...

Beam elements

Arbitrary cross-section of line-elements can be defined for Class-I and Class-II beam elements. Now this option is also available for Class-I beam elements. This option allows the user to specify an arbitrary cross-section with a number of quadrilateral (not necessarily rectangular!) zones. For class-I beams the zone information is used to compute the moments of inertia I_z , I_y , I_{yz} , and I_t . Note that average torsional shear stresses for class-I beams can only be computed during post-processing if the torsional rigidity W_t is specified.

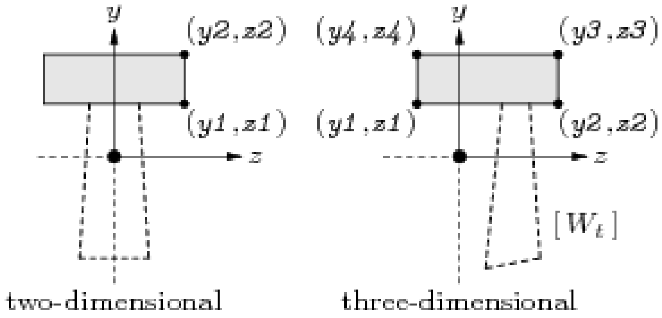

Cross-section definition of beams with zones

Curved shell with drilling rotations

A new class of curved shell elements with drilling rotation has been created by enhancing the existing linear and quadratic curved shell elements with an additional rotation φ_z, the drilling rotation. In applications where the elements are nearly co-planar in the nodes, the use of shell elements with drilling rotation is very attractive because they avoid an ill-condition of the assembled global stiffness matrix.

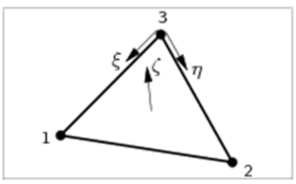

T18SH

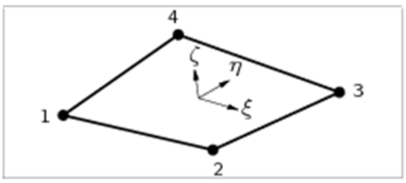

Q24SH

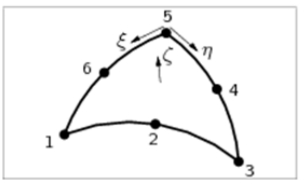

CT36S

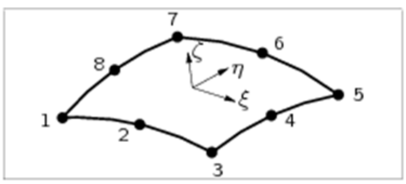

CQ48S

Bond-slip reinforcements in 2D and shell elements

Bond-slip reinforcements are now also available as embedded lines in plane stress and curved shell elements. In this case, the reinforcement bar is internally modelled as a truss or beam elements, which are connected to the mother elements by connection interface elements. Bond-slip reinforcements may be applied for modelling slip of steel reinforcement in concrete of for modelling interaction of pile foundations in soil and rock.

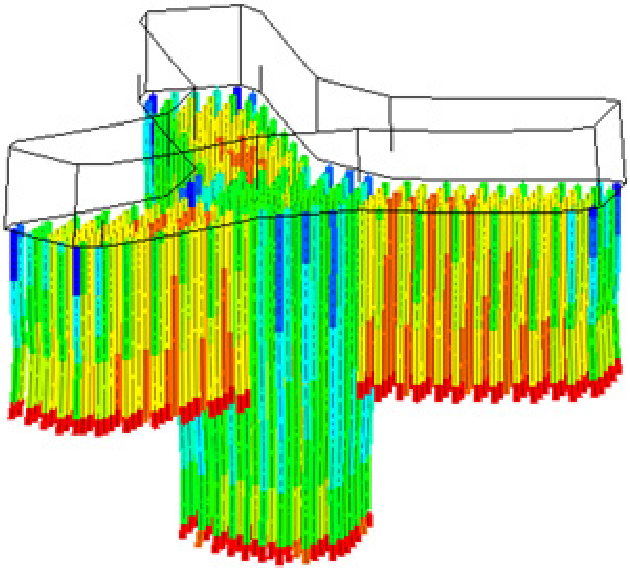

Axial forces in piles in pile-raft foundation

Boundary surface elements

DIANA has been extended with boundary surface elements. These line and surface elements replace the translational distributed mass elements and may be applied to add mass and/or stiffness properties to an outer surface of a finite element model. These elements may be applied either to add distributed mass to a finite element model without influencing the stiffness of the model, or to model the free field medium in a dynamic analysis. Line boundary surface elements are to be placed on the outer edge of a two-dimensional model or on the upper face of a line interface element. Plane boundary surface elements are to be placed on the outer surface of a three-dimensional model or on the upper face of a plane interface element.

Fluid-structure interface elements

Next to the quadratic and quadratic-linear fluid-structure interface elements linear fluid structure interface elements have been made available in DIANA. The BL4S2 element is a fluid-structure line interface element to be placed between the edges of two-dimensional linear structural elements and two-dimensional linear flow elements. BQ12S4 and BT9S3 elements are fluid-structure plane interface elements to be placed between the faces of linear solid (three-dimensional) structural elements and three-dimensional linear flow elements.

Composed line elements

DIANA has been extended with composed line elements. Composed line elements do not contribute to the force transfer in the finite element model, but can be used to calculate and check the cross-section forces and bending moments in the model. Cross-section forces and bending moment can be used to check correct loading and boundary conditions of the model, or whether a nonlinear analysis has reached the required accuracy. Both linear and quadratic composed line elements are available.

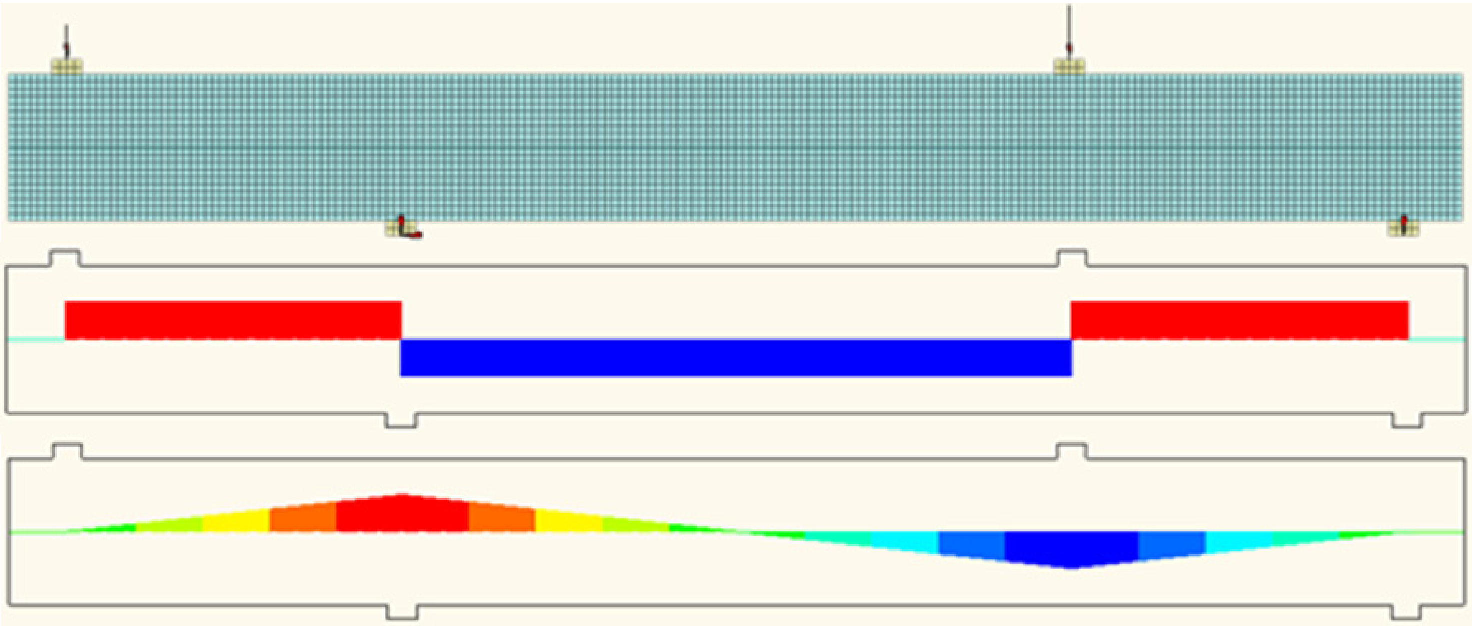

Reinforced concrete beam modelled with membrane elements. In composed lines the shear-forces diagram and the bending-moment diagram are displayed

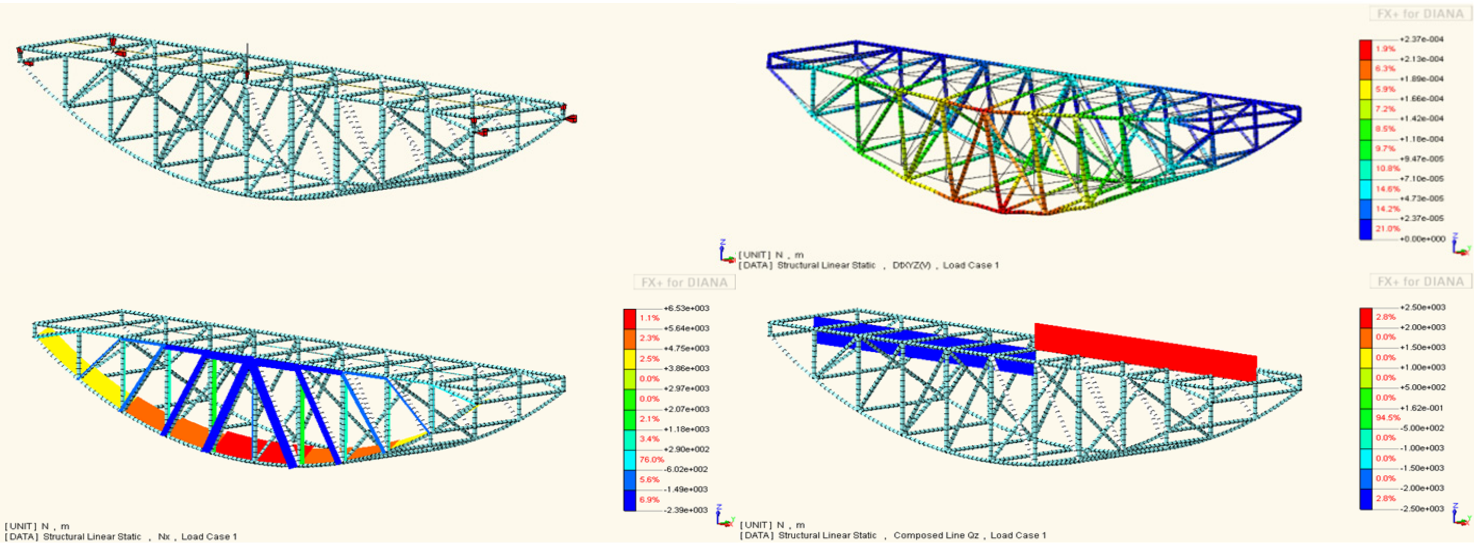

Bridge structure with beam-elements with a central eccentric point-load. Deformed shape, axial forces in individual member and shear-forces in composed line are displayed

Pre-stressing and post-tensioning of embedded reinforcements

The Korea Road & Transport Association-BRG2K highway bridge design standard can now also be used for preprocessing of pre-stress for post-tensioned reinforcement in bars and line-shaped grids (grids in plane strain or axi-symmetry), next to the already existing European CEB-FIP 1990 model code.

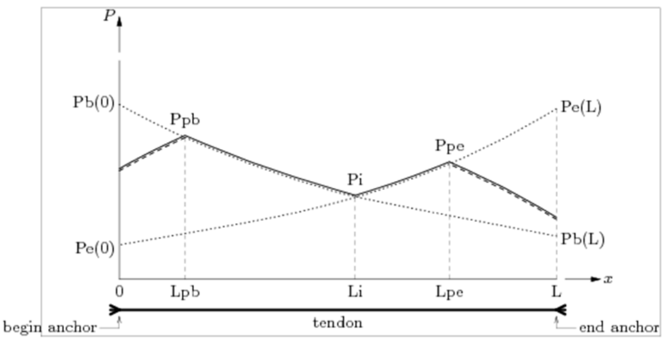

Intersection curves and limited penetration of both anchors

Tension cut-off for Mohr-Coulomb and Drucker-Prager

In earlier versions tension cut-off for soil models was modelled by cracking behavior. For Mohr-Coulomb and Drucker-Prager plasticity models now it is possible to specify an optional tension cut-off surface which is integrated in the soil model and behaves more robustly, because different return-mapping is applied for zone of axial return and zone of tensile-corner return. The tension cut-off surface limits the tension to a cut-off value of P_t.

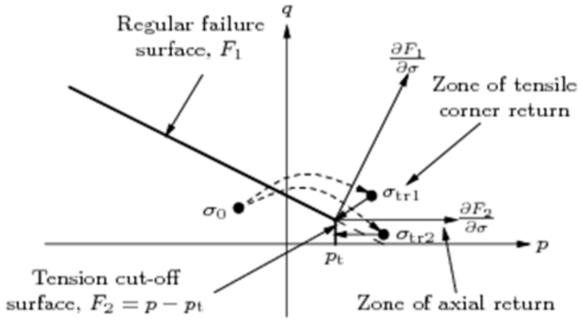

Tension cut-off surface for Mohr-Coulomb plasticity model

9.4.4. In more detail...

Engineering input for modified Mohr-Coulomb

A special version of the Modified Mohr-Coulomb model has been made available to the user. This special version of the Modified Mohr-Coulomb model allows the user to specify engineering parameters which are translated into standard parameters for the general Modified Mohr-Coulomb model with power-law nonlinear elastic behavior, exponential cap-hardening with Rowe's dilatancy rule and a parabolic hardening of the friction angle as function of the plastic shear-strain according to Duncan-Chang.

Extensions to total strain crack model

DIANA now offers the possibility to overrule the default values for parameters n and k of the Thorenfeldt compression curve for total strain based crack models. This also implies that Eurocode 2 input, which requires n = 3 , has become available.

Furthermore, DIANA now offers the ability to take the Poisson effect in cracked state into account. In a cracked state, the Poisson effect of a material ceases to exist. Stretching of a cracked direction does no longer lead to contraction of the perpendicular directions. To model this phenomenon, an orthotropic formulation is adapted for Poisson's ratios. Similar to a damage formulation where the secant modulus reduces after cracking, the Poisson's ratios reduce at the same pace.

(syntax)

```
'MATERI'
1    5 6    12 13                                                    80
     YIELD      MMC
     YLDVAL     e50r  eurr  eoedr  cr  phir  phi0r  psir  [ rfr  mr ]
    [PREF       prefr]
    [POISON     nur]
    [POROSI     nr]
    [KNC        kncr]
    [K0         k0r]
    [CAP        [alphar]]
    [SHPFAC     [beta1r [, beta2r]]]
```

Syntax for definition of modified Mohr-Coulomb material model with engineering input

Solidification or evaporation

DIANA now offers the possibility to specify a second enthalpy curve for materials that show a different capacity on cooling down and reheating than on the first heating. The cooling and heating capacity may be specified through the `ENTCOO` curve. This `ENTCOO` curve is defined additional to the specified `ENTHAL` curve. Whenever the temperature in a point is below the maximum experienced temperature in that point, the capacity is derived from the `ENTCOO` instead of from the `ENTHAL` curve.

D-min soil model

A new simple soil model is available in DIANA: The D-min model is a stepwise linear elastic isotropic model in which every load step the Young's modulus and Poisson's ratio are adapted. In this model the elastic parameters are defined as function of the relative difference of the stress at the beginning of the load step to the failure stress criterion. In a load step the material parameters are kept constant and therefore, this model does not need iterations. The D-min model can be applied in plane strain, axisymmetric, and solid elements.

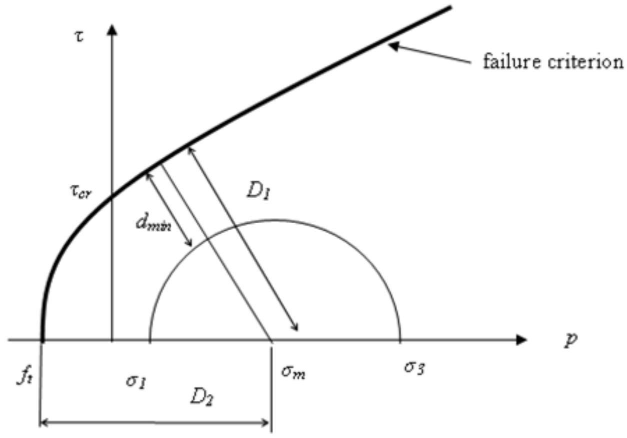

Definition of D-min parameter in stress-space

Classic Brick model

The Brick model is a strain-based constitutive relation for soil, initially presented by Simpson and has been further developed at different organisations in the UK. DIANA has been extended with the Classic Brick model. Soil particles tend to continue plastic deformation in the direction of their approach path immediately after change of the deformation direction. The Classic Brick model captures this phenomenon, this can be explained by the analogy of a person pulling bricks on strings. In this analogy the person corresponds with the current strain point and each brick moves in the direction of the string, this represents a proportion of the material behavior.

Modified 2-surface model for cyclic behavior of steel

DIANA has been extended with the modified two-surface model, which can treat the cyclic behavior of structural steels with the inclusion of the yield plateau. It consists of two surfaces: the yield surface as the inner surface and the bounding surface as the outer surface. The yield surface is always enclosed by the bounding surface and the value of the plastic modulus is determined by the proximity of the two surfaces in the course of their coupled translation and changes in size during plastic deformation.

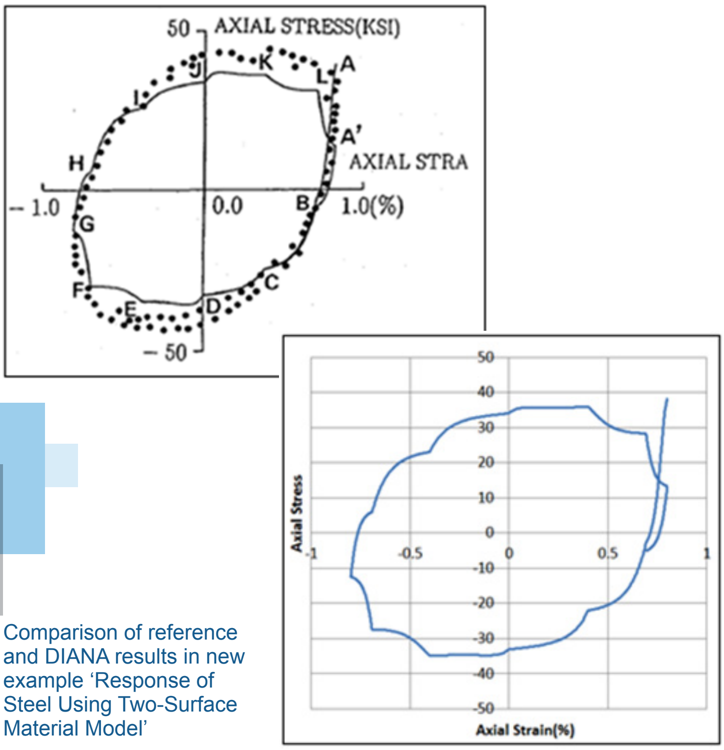

Comparison of reference and DIANA results in new example ‘Response of Steel Using Two-Surface Material Model’

Menegotto-Pinto plasticity model for cylic loading of steel reinforcements

The Menegotto-Pinto model is a special plasticity model for the cyclic behavior of steel. The Menegotto-Pinto model has the same basic expression as for the Monti-Nutti model. The difference between the models is in the hardening rule in relation to the load cycles. The Menegotto-Pinto model is available for embedded reinforcements.

Van Genuchten Relative Conductivity Function

DIANA now offers the possibility to determine pressure head dependent relative conductivity by a Van Genuchten function next to the Gardner’s coefficient function and a Frontal function. This is popular relation for groundwater flow analysis.

Using User-supplied Subroutines

DIANA now offers the possibility to use user-supplied subroutines from a precompiled library file. The file name of the library must contain the extension .dll on MS-Windows systems and .so on Linux systems. With this extension it is no longer required to use the same compilers as has been used for the standard DIANA code. The practical application of this option is explained in a USS white paper that can be downloaded from the http://tnodiana.com website.

Element Evaluation

DIANA has been extended with an averaging procedure on the nodal normals of all curved shell elements attached to a node if neither a predefined shape nor explicit thickness vectors are specified for the curved shell elements. This method leads to more accurate results for models with curved surfaces for which the underlying shape is unknown.

Linear constraints for flow analysis

Flow analysis has been extended with general linear constraints. Table ‘`EQUAL`’ has been replaced by the more general table ‘`TYINGS`’, which was already available for structural and coupled analysis. This option is useful for an excavation analysis in which groundwater levels are calculated before and after a pile-sheet wall is installed.

Prescribed accelerations

Prescribed accelerations have been made available as loading for transient dynamic analysis (`*NONLIN`). Prescribed accelerations can be used for modelling non-uniform nodal accelerations and are input in subtable `ACCELE` of table `LOADS`.

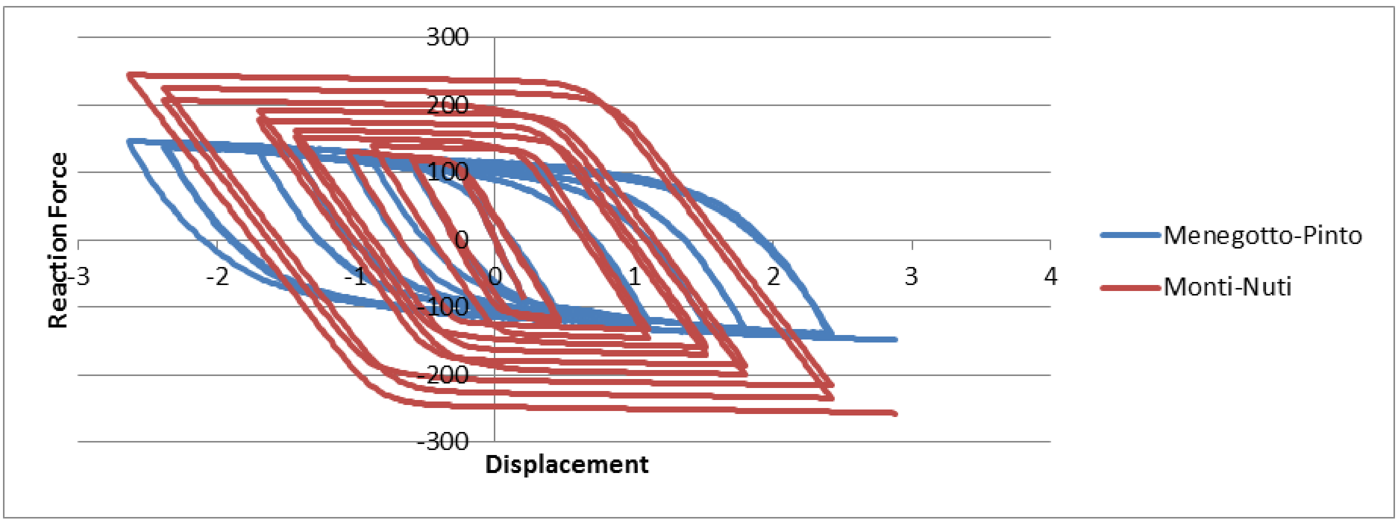

Comparison of response for Menegotto-Pinto and for Monti-Nuti model

9.4.4. In more detail...

Geometrical nonlinear analysis

Geometrical nonlinear analysis using the Updated Lagrange formulation is now also available for three-dimensional membrane elements and three-dimensional cable elements. In earlier versions the Update Lagrange formulation was already made available for beam and shell elements and for the regular plane strain, plane stress, axisymmetric and solid elements.

Arc-length control

Arc-length methods may now also be used in combination with prescribed non-zero displacements. Prescribed non-zero displacements and nodal or element loads, however, may not be applied in the same load set.

Logging

The logging information that will be output during execution of steps for structural nonlinear analysis has been extended with cumulative reaction forces and moments. This extension allows the user to do an easy check on loadings applied to the model at every load-level.

Damping and inertia forces

The linear and nonlinear transient dynamic analysis, and hybrid frequency time domain analysis procedures have been extended with nodal and element nodal damping and inertia forces as output item.

Euro-code 8 elastic and design spectra

For the direct frequency response, modal frequency response, and spectral response analysis procedures, frequency-load diagrams according to the elastic response spectra and the design spectra of Euro-code 8 can be used.

Transient dynamic analysis

The linear and nonlinear transient dynamic analysis procedures have been extended with the possibility to define the dynamic response due to an applied base acceleration in a relative coordinate system with respect to the base. When a relative coordinate system is used, no damping energy due to the base movement is added into the system when Rayleigh damping is being used.

Spectral response analysis

When the user requests superposition according to the Complete Quadratic Combination (CQC) rule in a spectral response analysis the correlation factors among the eigen-modes are written to the standard output file `file.out`.

Strength reduction analysis

A strength reduction method has been made available in DIANA. In this strength reduction method, the strength characteristics of the structural materials are reduced by a factor until the loss of stability, or until failure of the structure occurs. The reciprocal of this reduction factor is identified as the factor of safety associated with the structure under investigation. In DIANA this method is implemented as a separate module named `*REDUCT`. The main output of this analysis type is the factor of safety.

A typical use of this strength reduction method is the assessment of slope stability where dominantly a Mohr-Coulomb or similar material model is used. Therefore, cohesion (c) and/or friction angle (φ) are reduced to assess the slope stability. Presently in DIANA Mohr-Coulomb and Drucker-Prager models are considered for strength reduction analysis. Future extensions may include Modified Mohr-Coulomb, Hoek-Brown, and Coulomb friction (for interface elements) models.

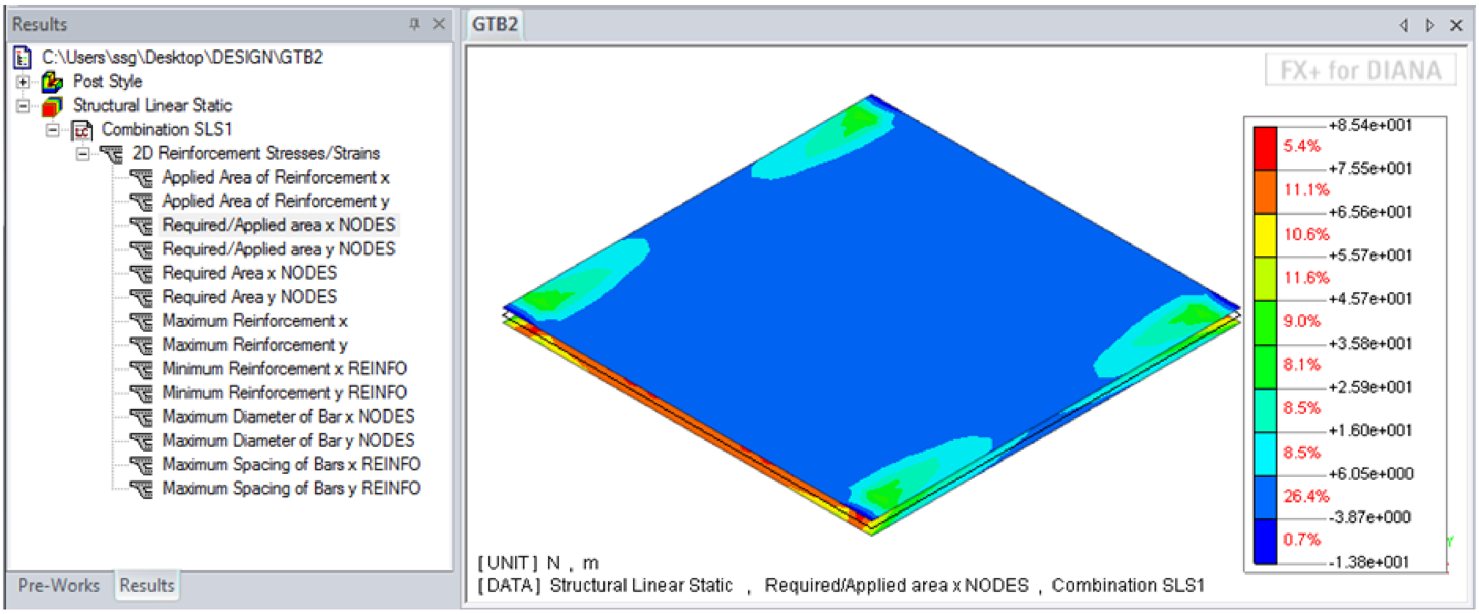

Design check results for a simple support plate

Reinforcement grid design checking

DIANA has been extended with reinforcement grid design checking. The *DESIGN application allows the user to perform the most important design checks with respect to reinforcement grids in concrete structures in the same finite element model that can be used for a nonlinear failure analysis of the structure. The reinforcement grid design checking application offers an option to output average values for the result items. If AVERAG is specified, for each node in a grid and for each result component in the direction normal to result component direction, a line with a length specified by the user is defined. The average results over the reinforcement particles that are intersected by this line are calculated and displayed in the node.

Stiffness adaptation analysis

Stiffness adaptation analysis is a new application for calculation of crack patterns and crack openings in an efficient and user-friendly way. The stiffness adaptation analysis performs a sequence of linear analyses in which in every iteration the stiffness is locally reduced automatically when the stress in the previous iteration was beyond the user-defined ultimate stress-strain curve. This method is efficient for predicting cracks, plasticity onset, force distribution and deformations in serviceability limit state analysis. A special white-paper on Stiffness Adaptation analysis is being prepared and can be downloaded from the http://tnodiana.com web-page.

Crack-width results

The nonlinear static and transient analysis procedure has been extended with crack width as output item. Crack width is defined as the product of the crack bandwidth h_{cr} and the summed crack strains of an element. Crack width can be output in an integration point or in a node and can be exported in the local, or the global coordinate system, or as principal crack width, or Von Mises crack width.

CAD based reinforcements

New commands have been added to simplify reinforcement creation based on CAD input. The following commands create reinforcements based on geometry that was imported:

- GEOMETRY TRANSFER LINE creates a reinforcement section at the location of the specified line and adds it to a reinforcement. It is also possible to input sets of lines that all need to be transferred to reinforcement sections in a reinforcement.
- GEOMETRY TRANSFER SURFACE creates a reinforcement section at the location of the specified surface and adds it to a reinforcement. It is also possible to input sets of surfaces that all need to be transferred to reinforcement sections in a reinforcement.

Labelling and colouring reinforcements

New commands have been added to visualize the DIANA element types and reinforcement particles in the result environment of iDIANA:

- LABEL MESH VARIANTS enables you to label all elements with the DIANA element type name. Reinforcement particles are labeled with their keyword BAR or GRID followed by their reinforcement number.
- VIEW OPTIONS COLOUR VARIANTS enables you to color all regular elements green and reinforcement particles orange.
- CONSTRUCT SET APPEND VARIANTS enables you to append elements of the specified variant, i.e. DIANA element type or reinforcement, to the set.
- CONSTRUCT SET REMOVE VARIANTS enables you to remove elements of the specified variant, i.e. DIANA element type or reinforcement, from the set.

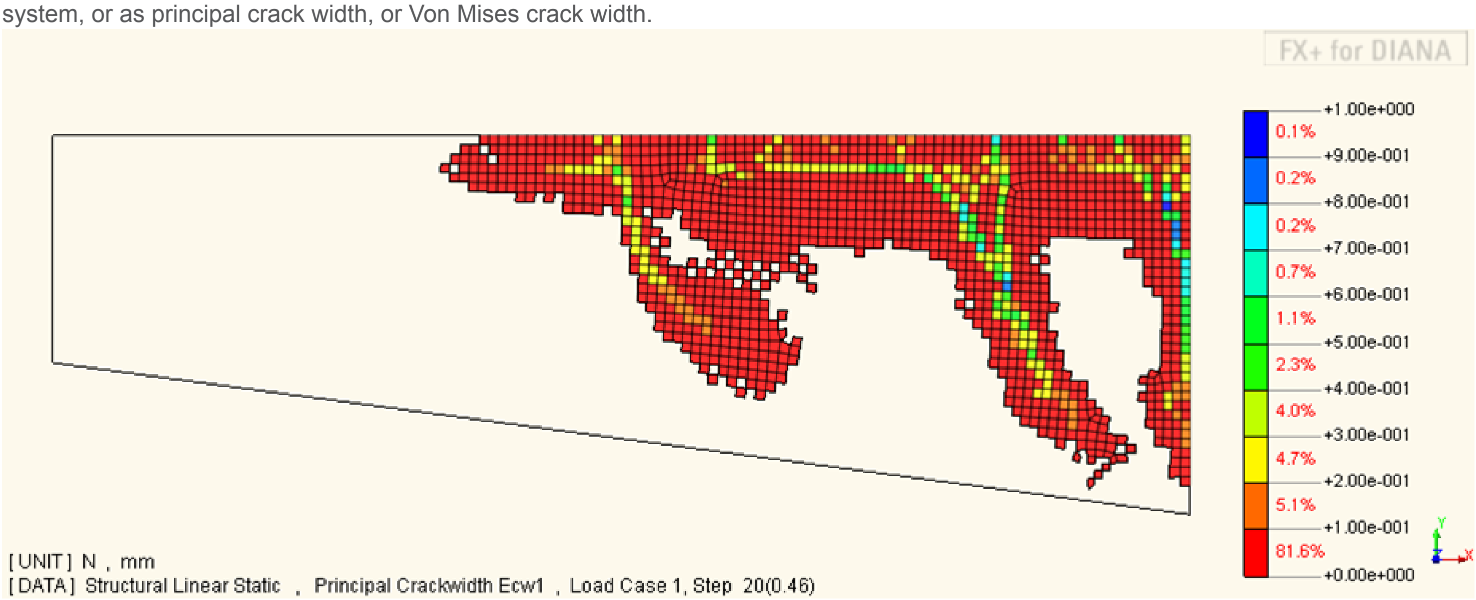

Crack-width result for eccentric reinforced concrete beam

Importing external files

CADfix is an external library integrated in iDIANA for import and repairing of CAD-models defined in several formats. The CADfix library has been updated to version 8.0, supporting many new releases of CAD programs.

Colour and style of vector plots

When the PRESENT OPTION VECTOR MODULATE ZERO is used in combination with a developed view, a vector scale bar will be displayed with a length of circa 5 % of the width of the viewport with the associated value being displayed.

9.4.4. In more detail...

Material properties

FX+ has been extended with the possibility to define material properties as text input. Text input should be defined in the same format as the 'MATERI' table in the DIANA data-file. Text input materials will be saved in the FX+ model file and be interpreted by DIANA. This option makes the full DIANA material options available in FX+, without the need to do adaptations in materials in MESH EDITOR.

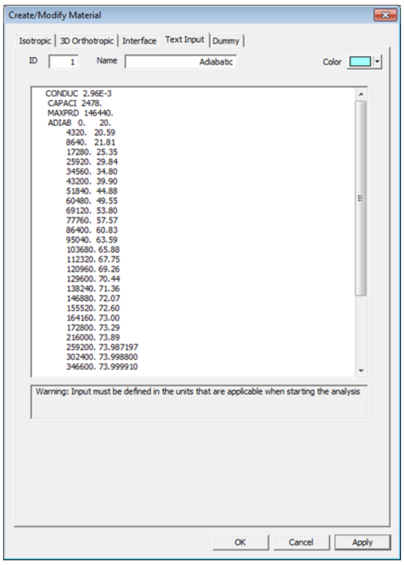

Text material input in FX+

Reinforcement sets

Reinforcement sets of FX+ are now also transferred to DIANA. In DIANA the reinforcement sets will appear as reinforcement groups in table 'GROUPS'.

Running DIANA

FX+ now offers the possibility to either directly run a DIANA analysis, when no modifications to the model are required and a DIANA command file is already available, or to define DIANA analysis commands without modifying the model in the MESH EDITOR, or to modify the FX+ model in the MESH EDITOR. This functionality offers the user quicker ways to start the analysis from FX+. Command-file specifications are not saved in the FX+ model-file.

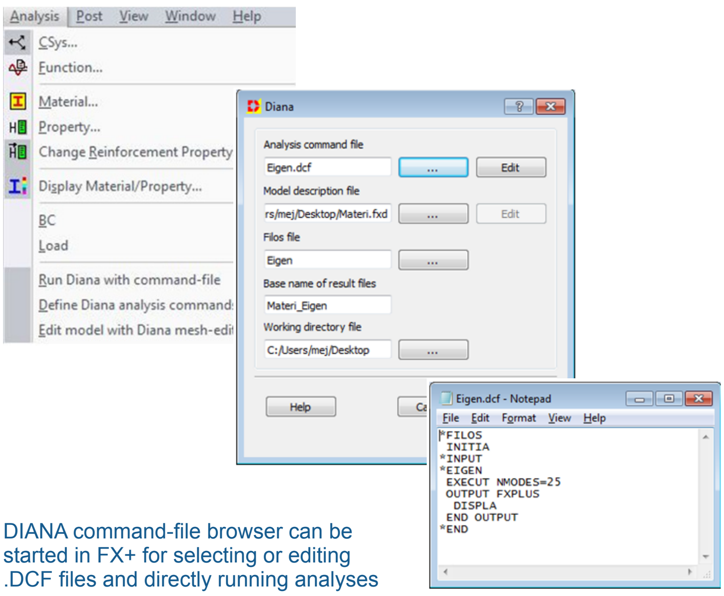

DIANA command-file browser can be started in FX+ for selecting or editing .DCF files and directly running analyses

Center or element and integration-point results

In earlier versions of DIANA, apart from status results and crack patterns FX+ results were always extrapolated to the nodes of elements. In cases where constant results per elements were sufficient, this extrapolation resulted in unnecessary large result files. In other cases this extrapolation resulted in overshoots which made it impossible for the user to check the values of the exact results in integration points against material model limits such as yield value or tensile strength. In this DIANA version the user may specify the location parameters NODES, INTPNT, and CENTER for the FX+ output device for results in nodes of the element, integration point results mapped to nodes, and averaged results per element, respectively.

Embedded reinforcement results

For embedded reinforcements it is now possible in FX+ to visualize the displacement results. This also implies that embedded reinforcement results can be displayed in a deformed mesh.

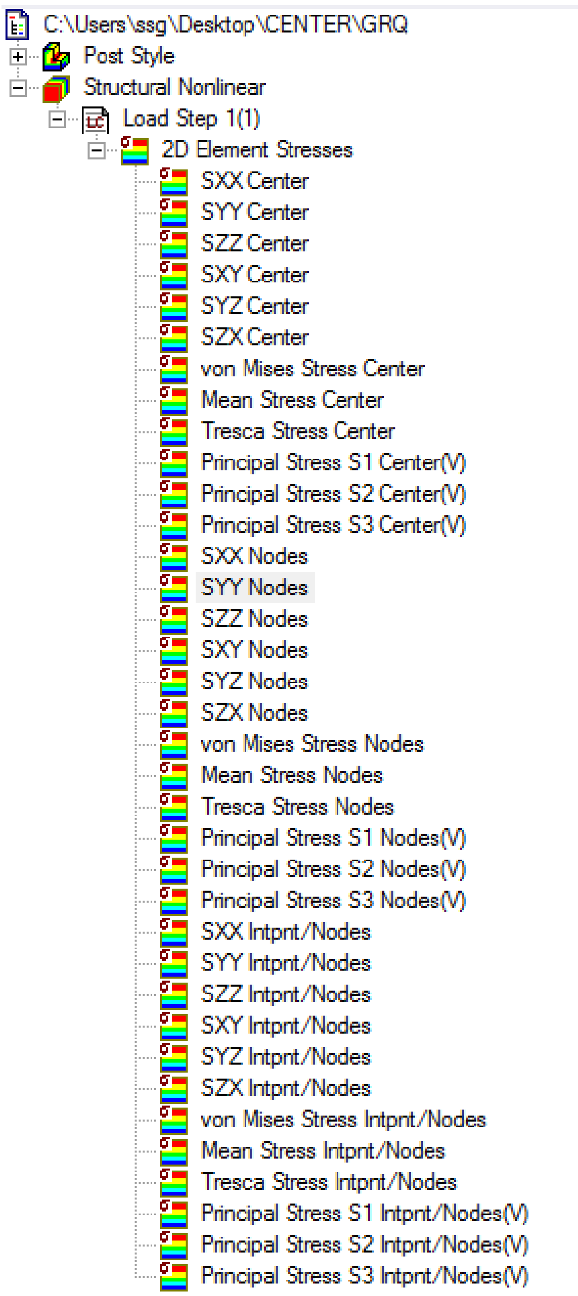

Element results such as stresses can now be output in the Center, in the Nodes or in the Integration points of Elements in FX+

Evaluation of the risk of cracking in thin concrete walls due to hydration heat

Authors: C. Zanotti & G. Plizzari, University of Brescia
A. Meda, University of Rome
S. Cangiano, CTG-Italcementi Group, Bergamo, Italy

In a wide range of concrete constructions, hygrothermal phenomena such as shrinkage or thermal variations can cause early-age cracking and thus compromise the structure performance. A numerical study on the risk of cracking induced in thin walls by thermal gradients during concrete hardening is presented in this paper. Heat produced by the reactions for cement hydration causes the development of thermal gradients that, combined to the low strength of concrete at early ages, can induce cracking. Thin concrete walls are strongly exposed to the risk of thermal cracking due to both the low thickness and the large size. Phased nonlinear heat transfer and structural analyses are performed in order to determine the solutions that can be adopted in practice to minimize the risk of cracking.

1 Introduction

Durability of concrete structures can be partially compromised by the unexpected cracking occurring a short time after casting. As a matter of fact, past negative experiences and investigations demonstrated that, in a wide range of constructions, severe cracks can develop due to hygrothermal phenomena of concrete, such as shrinkage and thermal variations (ACI 1993, Springenschmid 1995, Cusson & Repette 2000, Dere et al. 2006). In these cases, a thorough design of the structure and the construction phases is required in order to achieve long-term high structural performances.

During concrete hardening, cement hydration produces heat that causes the temperature rise. Because of the lower temperature of the surroundings, thermal gradients and, as a consequence, tensile stresses develop. Tensile stresses, combined to the low strength of concrete at early ages, could induce cracking (Springenschmid 1995). Concrete walls are particularly exposed to the risk of early-age cracking due to both their large size and low thickness (Kjellman & Olofsson 2001).

A numerical study on the risk of cracking in thin concrete walls due to the heat development during hydration is presented in this paper. The main scope of the study is to determine the solutions that can be adopted in practice to minimize the risk of cracking. To this purpose, coupled nonlinear flow-stress analyses are performed in order to assess the influence of different parameters, such as the mix-composition, the type of formworks and the construction phases on concrete cracking. In order to model the different construction phases and keep, at the same time, the continuity of the global behavior, phased analyses are performed.

2 Case Study: Geometry & Materials

The case study is a long concrete wall having the cross section geometry shown in Figure 1a. The wall height and thickness are equal to 5 m and 0.5 m, respectively. The wall is placed on a concrete slab foundation resting on soil and having a width of 1.5 m and a thickness of 0.5 m. For concrete casting, two different types of formworks are considered; the first type is a common 20 mm thick wooden formwork, while the second type is a 5 mm thick steel formwork, which represents the case of very low insulation between concrete elements and surroundings. An ambient temperature of 22°C is assumed.

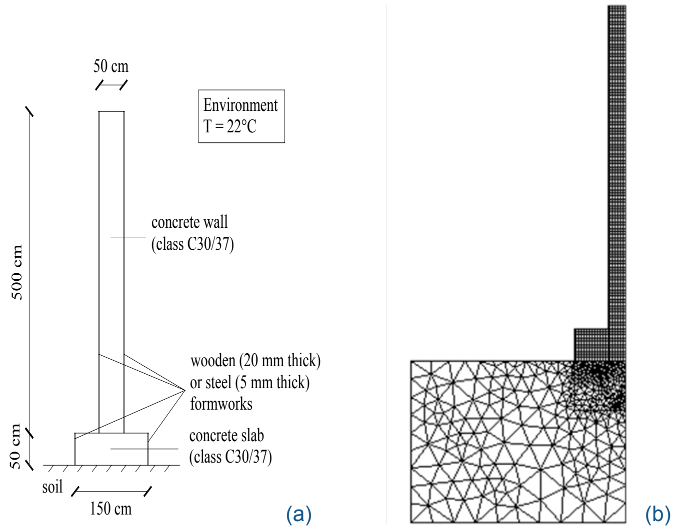

Figure 1. Reference geometry (a) and (b)

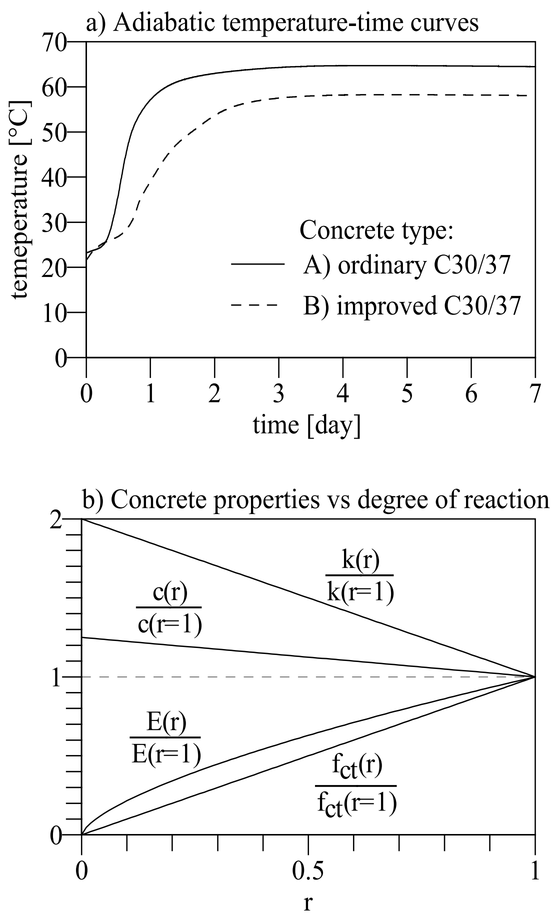

Figure 2. Experimental adiabatic temperature-time curves of concrete C30/37(a) and variation of thermal conductivity, k, specific heat, c, Young Modulus, E and tensile strength f_{ct} with the degree of reaction (b)

By reference to the European standards (EC2 2005), a concrete class C30/37 is assumed. Provided that, by varying the mix composition, the heat development during hydration varies, two different mix designs were developed: a common concrete having ordinary components, and a concrete improved by adding blast furnace slag, which limits the heat production. In order to assess the amount of heat produced during hydration, experimental tests were performed. Cubic specimens were insulated by means of polystyrene layers and the temperatures developed during the first week after casting were monitored. The experimental adiabatic temperature-time curves are shown in Figure 2a.

The influence of the construction process on the risk of cracking is analyzed by varying the time span between the slab casting and the wall casting as well as the time exposure of formworks.

3 FE ANALYSIS

FE phased analyses are carried out by means of DIANA FE program (release 9.3, Manie & Kikstra 2008a). In the case of contemporary casting of the slab and the wall, the construction process is divided into two phases: casting of concrete elements and removal of formworks (2, 4 or 6 days after casting). In the case of non contemporary casting, four construction phases are considered: slab casting, removal of slab formworks (2, 4 or 6 days after slab casting), wall casting (7, 14 or 28 days after slab casting) and 4) removal of wall formworks (2, 4 or 6 days after wall casting), as sketched in Table 1.

Initially, nonlinear heat transfer analyses are performed in order to study the hardening process and thus determine the development of temperature induced by the hardening process with time. Eventually, these results are adopted as input data for structural analyses. Besides thermal gradients (induced by hydration), only the dead load is applied on the structure during concrete hardening process.

For heat-transfer analysis, the unknown degree of freedom of the equation for global heat transfer (Equation 1) is temperature.

$$\rho c \frac{\partial T}{\partial t} = \nabla (k \nabla T) + q \quad (1)$$

where T is temperature, t is time, ρ is the material density, c is specific heat, k is thermal conductivity, ∇ is the spatial gradient and q is the amount of power that is generated (by hydration in this case).

Provided that, in the case of long slim elements, thermal gradients mainly develop along the cross section, a plain-strain two-dimensional model is adopted (Figure 1b). Concrete parts are modeled by means of quadrilateral isoparametric elements, having a size of either 40x40 mm or 40x10 mm. Triangular isoparametric elements are used for soil. The integration scheme is quadratic for structural analysis and linear for heat-transfer analysis so that compatibility between displacement and temperature formulations is guaranteed.

Two-node boundary elements are placed along the perimeter to model convection. Adiabatic conditions are imposed along the vertical axis of symmetry of the cross section and both the lower and the lateral edges of soil (where the diffusion process is supposed to be exhausted).

Horizontal translational constraints are applied along the lateral edge of soil and the vertical axis of symmetry, while vertical translational constraints are placed along the lower horizontal edge of soil.

	Contemporary casting	Non contemporary casting
Phase 1	Casting of concrete elements	Slab casting
Phase 2	Formwork removal *(2, 4 or 6 days after casting)*	Slab formwork removal *(2, 4 or 6 days after slab casting)*
Phase 3		Wall casting *(7, 14 or 28 days after slab casting)*
Phase 4		Wall formwork removal *(2, 4 or 6 days after wall casting)*

Table 1. Phases of the construction process

3.1 Hydration process

Concrete hardening and temperature development are reproduced by means of the nonlinear formulation proposed by Reinhardt et al. (1982). The degree of reaction is the parameter that accounts for the hardening stage of concrete and is defined by Equation 2.

$$r(t,x,y,z) = \frac{Q(t,x,y,z)}{Q_{\max}} \quad (2)$$

where t is time and x, y, z are the global coordinates, Q is the actual amount of heat that has been generated and Q_{max} is the total heat of hydration. Cement hydration is completed when r = 1.

The rate of heat evolution, q, is a function of the actual temperature, T, and the degree of reaction, r. According to Reinhardt et al. (1982), the function can be split in two parts, one depending on the degree of reaction and one depending on temperature only, as expressed by Equation 3; the well-known Arrhenius relation, here named $g(T)$, is commonly applied for modeling the influence of temperature on the rate of heat evolution.

$$\frac{\partial Q}{\partial t} = q\left(t,x,y,z\right) = g(T) f(r) = a \exp\left(-\frac{b}{T(t,x,y,z)}\right) f(r(t,x,y,z)) \quad (3)$$

where a and b are material constants.

In the present work, coefficient b (that is Arrhenius constant) is equal to 6000 (as usually assumed), while term $af(r)$, that is the adiabatic rate of heat evolution, is derived from the experimental adiabatic temperature-time curves shown in Figure 2a. As a matter of fact, for a given time increment, Δt, Equation 4 can be applied (Reinhardt et al. 1982, Manie & Kikstra 2008b).

$$af(r) = \bar{q} \exp\left(\frac{b}{T}\right) = \frac{c \Delta T}{\Delta t} \exp\left(\frac{b}{T}\right) \quad (4)$$

where c is the specific heat and $\bar{q}$ is the average rate of heat evolution within the given time increment, Δt.

Provided that function $f(r)$ is scaled to one, coefficient a takes the meaning of the maximum rate of heat evolution and is equal to the maximum value of term $af(r)$.

3.2 Thermal properties of concrete, formworks and soil

Thermal properties of concrete, wooden or steel formworks and soil are listed in Table 2; radiation is neglected at present. The 5 mm thick formworks are modeled by means of 20 mm thick elements (as for wooden formworks) having a fictitious thermal conductivity k^*. Provided that thermal conductivity within slender formworks mainly occurs along their thickness, the proper value of k^* is obtained by increasing the actual value of steel conductivity (Table 2) four times (since conductivity is linear and 20mm/5mm = 4).

Material	k [W/mK]	c[J/kgK]	h[W/m²K]	ρ[kg/m³]	E[MPa]	ν	f_{ct}[MPa]
Concrete*	1.19	900	25	2300	33000	0.2	2.9
Soil	1.1	880	-	1600	100	0.35	-
Wooden formwork	0.12	3780	4	300	-	-	-
Steel formwork	40	473	15.46	7900	-	-	-

* Concrete properties are referred to the case of hardened material at the lab temperature of almost 20°C

Table 2. Thermal properties: thermal conductivity, k, specific heat, c, convection, h, and density, ρ. Mechanical properties: Young Modulus, E, Poisson coefficient, ν, and tensile strength, f_{ct}

Concrete thermal properties are strongly affected by the degree of reaction, that is to say the hardening stage of the material, as well as by temperature. The linear functions proposed by Reinhardt et al. (1982) are adopted for modeling the influence of the degree of reaction on the thermal conductivity and the specific heat, as shown in Figure 2b.

Concerning the influence of temperature, reference is made to the European standards (EC2 2004). However, as Figure 2a shows, the maximum temperature is equal to almost 65°C in the worst case, while the minimum temperature is the ambient temperature, that is 22°C. Temperatures involved by hydration are therefore much lower than 100°C and vary within a limited range; as a consequence, all concrete properties (i.e. specific heat, thermal conductivity and density) hold steady, actually (Plizzari et al. 2009, Zanotti et al. 2009).

3.3 Mechanical properties of concrete and soil

Hardened concrete at ambient temperature has a tensile strength of 2.9 MPa and a Young Modulus of 33000 MPa (class C30/37, EC2 2005), as listed in Table 2. In Figure 2b, the development of the mechanical properties during concrete hardening can be observed. The tensile strength is assumed to be a linear function of the degree of reaction, r, while the Young Modulus is supposed to be proportional to $r^{2/3}$ (Onken & Rostàsy 1995, Eirle and Schikora 1999).

Soil is modeled as a linear elastic continuum, with a Young Modulus of 100 MPa and a Poisson coefficient of 0.35 (Table 2).

4 DISCUSSION OF THE FE RESULTS

4.1 Concrete hardening and development of temperature

Figures 3, 4 show the development of both temperature and the degree of reaction throughout the first days, in the case of non contemporary casting executed by means of 20 mm thick wooden formworks. The temperature rise in the slab is lower than the one in the wall due to the different geometry. A week after casting, the slab temperature already equals the ambient temperature (Figure 3a) and the hydration reactions are almost entirely exhausted at that time ($0.9 < r < 1$, Figure 3b). As a consequence, the different results obtained by varying the time span between the foundation and the wall casting from 7 to 28 days, agree.

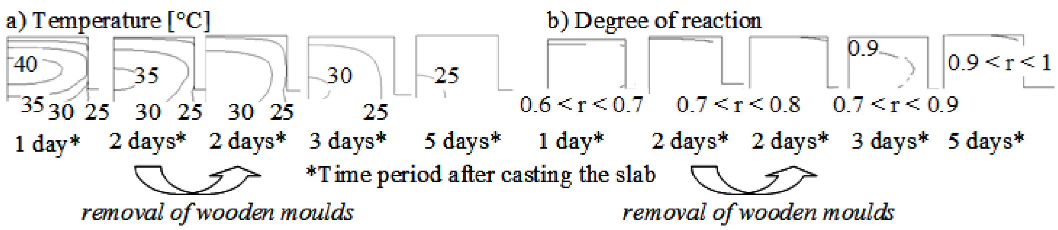

Figure 3: Temperature (a) and degree of raction (b) in the concrete slab throughout the first days, in the case of non-contemporary casting executed by means of wooden formworks

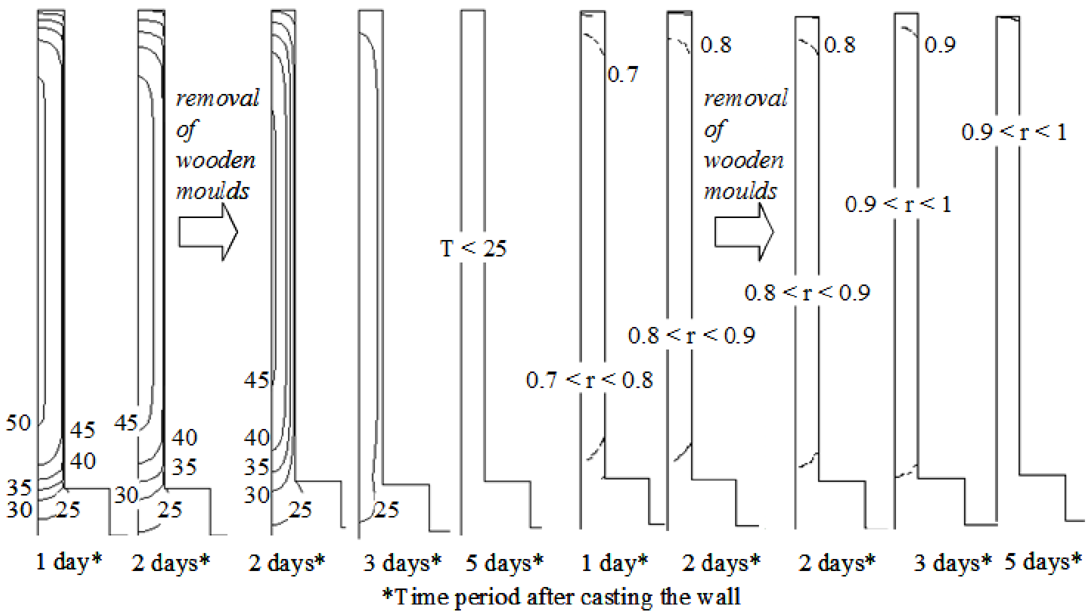

Figure 4: Temperature (a) and degree of reaction (b) in the concrete wall throughout the first days, in the case of non-contemporary casting executed by means of wooden formworks

At a given time, lower temperatures develop close to the edges of the concrete elements, due to the exchange of heat with the surroundings (Figures 3a, 4a); accordingly, the inner concrete parts harden faster than the external ones (Figures 3b, 4b). Therefore, a lower insulation from the surroundings provides higher thermal gradients within the cross section and a slower hardening process. Please note that the removal of wooden formworks, which provide a significant insulation, is followed by the sudden cooling of concrete elements and, most of all, of the lateral edges.

4.2 Risk of early-age thermal cracking

The risk of cracking χ is here defined as the maximum value of σ_I / f_{ct} ratio along the concrete element, with σ_I the maximum principal stress in a given point at each time and f_{ct} the tensile strength reached in that point at the same time. Cracks conventionally appear when χ=1; however, the first cracking is usually associated to a value of 0.7 as safety condition.

Figure 5 shows the development with time of the crack risk in the wall obtained by assuming that the wall is cast at least a week after the foundation. Either steel or wooden formworks are adopted and the laying time of formworks is varied from 2 to 6 days. According to the numerical results, wooden formworks are able to prevent the wall cracking, since the maximum crack risk, which is reached about one day after casting, is lower than 0.7 (point A, Figure 5a). However, if formworks are removed too early (as an instance, two days after casting), that is, when concrete temperatures are still high, the sudden cooling shown in Figure 4a causes surface cracking (point B, Figure 5a). The crack risk can be significantly reduced by postponing the removal of formworks from two to four days (point C, Figure 5a); moreover, thermal cracks could be completely avoided by extending the formwork laying up to six days (point D, Figure 5a).

Steel moulds provide lower insulation in comparison with wooden formworks and thus high thermal gradients develop within the wall thickness. As a consequence, the crack risk, , turns out to be higher than 1 a few hours after casting (point A, Figure 5b). Provided that a lower amount of heat is accumulated during the laying of steel moulds, the removal of steel moulds causes just a slight increase of the crack risk (points B, C, D, Figure 5b).

Please note that two very different types of crack may appear (Figure 6a). The early removal of well-insulating formworks could produce surface cracks, whereas more damaging throw cracks could develop in the core of the cross section due to inadequate insulation straight after casting (Kjellman & Olofsson 2001). Therefore, the first crack type appears after the removal of formworks, while the second crack type appears before (a few hours after casting).

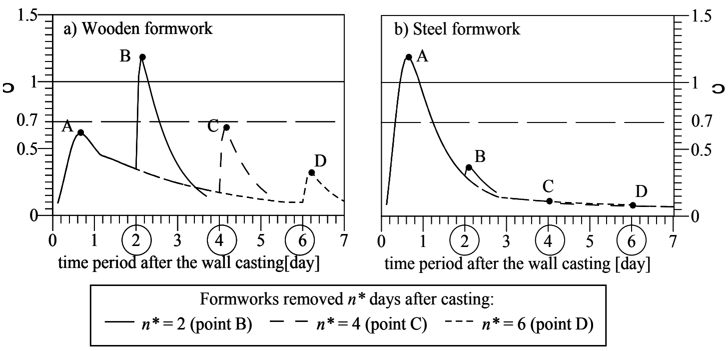

Figure 5: Risk of cracking (χ) in the wall through the first week after casting, in the case of ordinary concrete C30/37 (type A, Figure2a) and non-contemporary casting, executed by means of either wooden (a) or steel (b) formworks

In Figure 6b the maximum values of the crack risk obtained straight after casting as well as after the removal of formworks are compared for varying the following features: mould type, time period of mould laying, time span between the foundation and the wall casting (contemporary or not) and heat development during concrete hardening (i.e. the adiabatic temperature-time curves of Figure 2a). In the case of contemporary casting, a higher amount of material hardens at the same time and a higher amount of hydration heat is produced. Therefore, higher thermal gradients develop and thus the risk of cracking strongly increases on the whole. For ordinary concrete elements placed by means of steel moulds, the risk associated to the appearance of throw cracks before the mould removal increases from 1.2 to 2.4. Moreover, not even wooden formworks seem to be able to prevent throw cracks by themselves, since the crack risk χ equals 1.1 in ordinary concrete before the formwork removal.

A further consequence of casting the foundation and the wall at the same time instead of different moments is that a more significant cooling follows the formwork removal. As a result, a damaging increase in the risk of surface cracking can follow not only the early removal of wooden formworks, but also the removal of steel moulds. As a matter of fact, a crack risk equal to almost 1 is associated to the removal of steel moulds two days after casting. The laying time of steel moulds should be therefore extended up to at least four days in that case.

Cracking within the core of the cross section could be effectively prevented by improving the mix composition so that the heat development is limited during cement hydration. The addition of blast furnace slag in the concrete mix allows to both reduce and slacken the production of heat, as shown by the experimental temperature-time curves of Figure 2a, with the beneficial effect that the crack risk significantly decreases. As an instance, in the case of contemporary casting executed by means of wooden formworks, the crack risk is reduced from 1.1 to 0.65 (Figure 6b); the risk further decrease up to 0.35 in the case of non contemporary casting. On the other hand, the improvement of the mix composition does not wholly avoid surface cracking, even though the risk is slightly reduced. The removal of wooden formworks just two days after casting is followed by a crack risk equal to 1.3 or to 1, in the case of contemporary or non contemporary casting, respectively; wooden formworks should therefore lay for at least 3 or 4 days.

5 CONCLUDING REMARKS AND FUTURE WORKS

A numerical study on the risk of early-age cracking in thin concrete walls due to hydration heat was presented in this paper. The main results can be summarized as follows:

- Thin walls made of ordinary concrete are actually exposed to a significant crack risk, mainly due to the low thickness and the large size. However, the construction process can be improved with some simple expedients that might allow to prevent cracking. Moreover, particular components, such as blast furnace slag, can be adopted in order to both slacken and limit the heat development.
- A low insulation between the concrete wall and the surroundings induces a very high risk that dangerous throw cracks develop straight after casting. Therefore, well insulating formworks should be adopted; as an instance, wooden formworks should be preferred to steel moulds.
- The early removal of well-insulating formworks might cause surface cracking due the sudden cooling of the concrete wall. As a general rule, the laying time of wooden formworks should equal at least 4 days. The laying time can be reduced by adding blast furnace slag in the concrete mix.

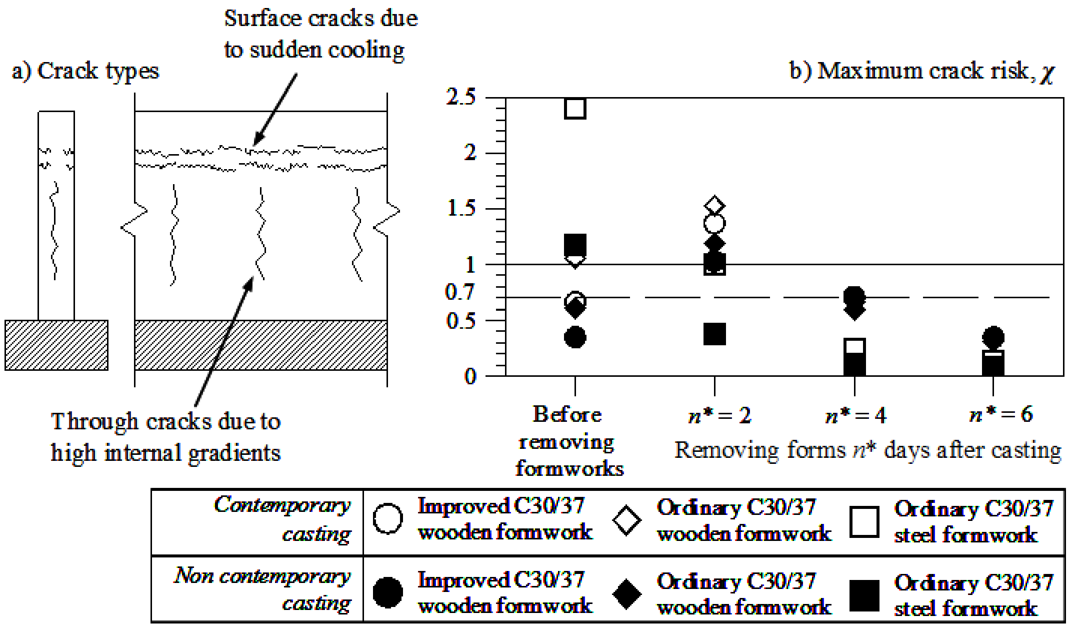

Figure 6. Different types of cracks that may appear (a). Maximum crack risk (b) obtained straight after casting as well as after the removal of formworks for varying: mould type, time period of mould laying, time span between the foundation and the wall casting (contemporary or not) and heat development during concrete hardening (Figure 2a).

- The risk of cracking is strongly affected by the global amount of heat that is produced during concrete hardening; therefore, in the case of large size, concrete elements should be divided in different parts, cast at different times. As an instance, the crack risk strongly increases in the case of contemporary casting of the wall and the slab analyzed in the present work.

Future development of the research will concern the effect of thermal creep on the risk of cracking in the wall.

6 REFERENCES

ACI 224.1.R-93. *Causes, evaluation and repair of cracks in concrete structures. American Concrete In-stitute.*

Cusson, D. & Repette, W. 2000. *Early-age cracking in reconstructed bridge barrier walls. ACI Materials Journal, July-August, pp. 438-446.*

Dere, Y., Asgari, A., Solentino, E.D. & Archier, G.C. 2006. *Failure prediction of skewed jointed plain concrete pavements using 3D FE analysis. Engeneering Failure Analysis, Elsevier, Vol.13, pp. 898-913.*

EC2 2004. *Design of concrete structures. Part 1-2: General rules – Structural fire design. EN 1992-1-2*

EC2 2005. *Design of concrete structures. Part 1-1: General rules and rules for buildings. EN 1992-1-1.*

Eierle, B. & Schikora, K. 1999. *Computational modelling of concrete at early ages using DIANA. DIANA World 2/99.*

Kjellman, O. & Olofsson, J. 2001. *3D structural analysis of crack risk in hardening concrete (verification of an engineering method. Report n. 2001:53-2. Luleå University of Technology, Department of Civil and Mining Engineering, Division of Structural Engineering.*

Manie, J. & Kikstra, W.P. 2008a. *DIANA – Finite Element Analysis. User's manual release 9.3. Analysis Procedures. Delft: TNO DIANA BV.*

Manie, J. & Kikstra, W.P. 2008b. *DIANA – Finite Element Analysis. User's manual release 9.3. Material Library. Delft: TNO DIANA BV.*

Onken, P. & Rostàsy, F. 1995. *Wirksame betonzugfestigkeit im bau-werk bei früh einsetzendem temperaturzawang, DAfStb Heft 449, Berlin: Beuth-Verlag.*

Plizzari, G., Meda, A. & Zanotti, C. 2009. *Studio numerico sul rischio di prematura fessurazione delle opere in calcestruzzo. Technical Report. University of Brescia, Department DICATA (in print). In Ital-ian.*

Reinhardt, H.W., Blaawendraad, J. & Jongendijk, J. 1982. *Temper-ature development in concrete struc-tures taking account of state dependent properties; Proc. of the International Conference of Con-crete at Early Ages, RILEM, Paris, 6-8 April 1982.*

Springenschmid, R. 1995. *Thermal cracking in concrete at early ages - Proc. of the International RILEM Symposium, Munich, 10-12 October 1994. London: E & FN Spon.*

Zanotti, C., Meda, A., Plizzari, G. & Cangiano, S. 2009. *Problem-atiche legate al rischio di prematura fessurazione delle opere in cal-cestruzzo; Proc. of the AICAP Conference, Pisa, 14-16 May 2009. In Italian.*

Prediction of Crack-width and Crack-pattern

Authors: Gerd-Jan Schreppers,
Chantal Frissen & Hee-Jeong Kang,
TNO DIANA BV

Introduction

Cracks in reinforced concrete structures are undesired because they:

- do not look good
- affect the durability of the structure
- lead to changes in stiffness and change force distribution in the structure
- give feeling that construction is unsafe

Due to the brittle nature of concrete and because of changing loading conditions and other factors which are not considered in the design (such as internal stresses resulting from casting), cracks in concrete infrastructures, eg. bridges, can never completely be avoided in practice.

Design-codes give guidelines for checking the amount of reinforcement that is required in a structure to keep the crack-width limited to a certain value at specified load-levels. Checks in design codes are mainly based on the forces and bending moments in the cross-section of the structure, and are unreliable for relatively thin plate-shaped structures, but are conservative for non-standard structures with more complex loading and support conditions. Further, design-codes do not give suitable guidelines for the assessment of seriously deteriorated existing structures, and in particular for how crack-widths and strength of such structures can be managed.

Full non-linear finite element analysis has proven to be able to predict accurately changing stiffness and crack-widths at different load-levels. However, it has not been accepted in engineering practice because such analyses take time and require certain expertise for getting useful results.

Stiffness Adaptation Method

The stiffness adaptation analysis with application *STADAP is proposed to be an alternative for a full nonlinear analysis with application *NONLIN for calculating load distributions, deformations, crack patterns, and crack-width in reinforced concrete structures.

A stiffness adaptation analysis performs a sequence of linear static analyses, wherein a subsequent iteration the elastic stiffness will be reduced in those integration points in which the stresses in a previous iteration were beyond a user-specified uni-axial stress-strain curve. In such a case the isotropic elastic stiffness model is changed into an orthotropic elastic stiffness model with a reduced stiffness in the direction of the maximum stress, such that, with the same strain in the integration point, the maximum stress will be mapped on the stress-strain curve.

In stiffness adaptation analysis both standard linear elastic material as well as nonlinear material behaviour can be defined. Nonlinear materials can be defined through a uni-axial stress-strain curve, both in the tensile and in the compressive regime. Nonlinear stress-strain curves may also be defined for bar and grid reinforcements.

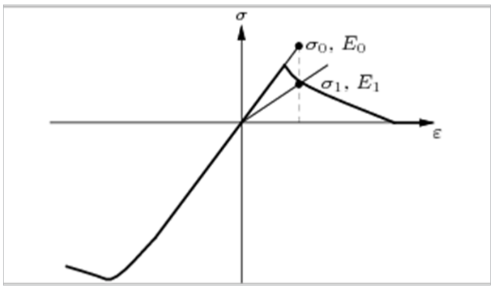

Figure 1. Uni-axial stress-strain curve with stress and stiffness reduction

Figure 1 displays that a maximum stress σ0 in an integration point is beyond the stress-strain curve. As a consequence, in the respective integration point and stress direction the stiffness E0 is reduced in the next iteration such that the related stress σ1 and corresponding stiffness E1 in this direction is located exactly on the stress-strain curve. Because of the local stiffness change, the deformation of the model will change in the next iteration. After a certain number of iterations for all the integration points in the model the stress-strain combinations will be on or below the user-defined stress-strain curve. DIANA applies a tolerance of 1% in the stress as criterion whether stiffness needs to be adapted or not.

In every integration point, two stiffness values are identified: one for the direction of the highest principal stress, and one for the direction of the lowest principal stress. In three-dimensional stress conditions, such as in solids and shell elements, for the stiffness in the direction of the second principal stress, the highest stiffness from the other two directions is applied. Initially the linear elastic stiffness is applied in all directions. The Poisson's ratio and shear stiffness are reduced with the same ratio at the maximum stiffness reduction in the respective integration point. The compressive strength is automatically reduced according to the relative ratio as defined by Vecchio and Collins as applied to the Total Strain crack model in DIANA, see Volume Material Library. The stiffness reduction is limited to 0.001 times the original Young's modulus.

In a stiffness adaptation analysis different loadings can be applied subsequently to simulate the loading history of the construction. Every loading can be applied in one step or in several steps with constant or varying step sizes. The user defines the maximum number of iterations per load step. If at a certain load level no further stiffness adaptations are required, because in all integration points the maximum stresses are within the 1% tolerance on or below the stress-strain curve, DIANA will stop the iteration process for that load step and continue to the next load step [Fig.2].

In a stiffness adaptation analysis the material status parameters can never be corrected in later iterations. This is in contrary to full non-linear analysis where the update of material status parameters is first confirmed at the end of a load step. Therefore, it is important to select the load increments carefully. If load increments which are too large are chosen when cracks develop in the model, the number of elements with stresses beyond the stress-strain curve will be large and the number of elements for which stiffness needs to be adapted is also large. In such situations large load increments may lead to

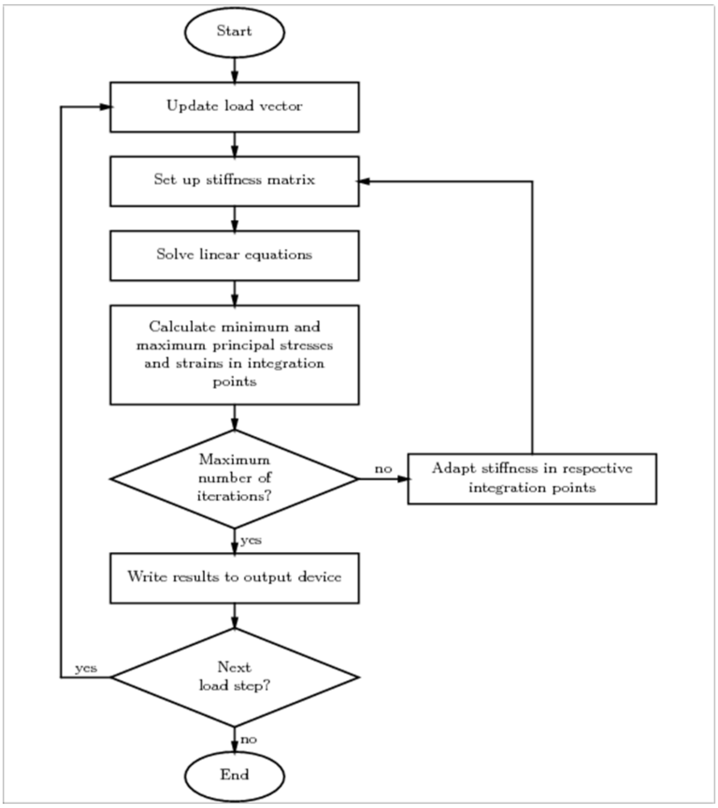

Figure 2. Flowchart of analysis sequence for stiffness adaptation

widely spread areas with stiffness reduction, whereas, when smaller load increments are defined, the damage or cracks will be much more localised, resulting in a single line of elements with reduced stiffness.

In many cases it is sufficient to limit the maximum number of iterations per load step to 10. Also because, if after this number of iterations there are further stresses beyond the stress-strain curve, these errors are usually small. In order to describe the load and damage history more accurately it is recommended to apply more and smaller load steps with a lower maximum number of iterations per load step than using fewer, but larger steps with a higher number of iterations per load step.

Stiffness adaptation analysis can be used efficiently for calculating load distributions in nonlinear structures, for deformations at different load levels, and for crack patterns and crack openings, as well as for plastic deformations in reinforcements. In comparison with full nonlinear analysis (*NONLIN) the analysis times of the stiffness adaptation method will be shorter, and no advanced analysis procedures and settings are required. Stiffness adaption analysis can effectively be used to predict cracks and crack openings in serviceability loading conditions. For ultimate limit state analysis and analysis with ambient influences the use of a full nonlinear analysis with application NONLIN is recommended.

Deep Reinforced Concrete Beams

Extended measurements of crack width in deep reinforced concrete beams performed by Braam at Delft University and reported in Heron [1] in 1990 were chosen as first reference for stiffness adaptation analysis results.

The mesh is defined with 4-nodes quadrilateral elements of 20*20 mm. Top-flange elements (yellow) have a thickness of 300 mm and web-elements (blue) have a thickness of 150 mm. For symmetry reasons only half of the beams were considered in the finite elements model. Measurements have been performed on different reinforcement configurations and corresponding models have been analysed. In this paper we only report analyses of Beam 1 and Beam 6. The 4 bars at the bottom of the web, with diameter of 20 mm, were modelled as 1 equivalent bar, with cross-section of 0.001257 mm2 at 70 mm distance bottom and for Beam6 the 2 bars, with diameter of 10 mm, in the middle area of the flange are modelled as 1 equivalent bar, with cross-section of 0.000157 mm2.

At the loading point and the vertical support point a steel plate of 180*40 mm is applied to spread the load and avoid local effects.

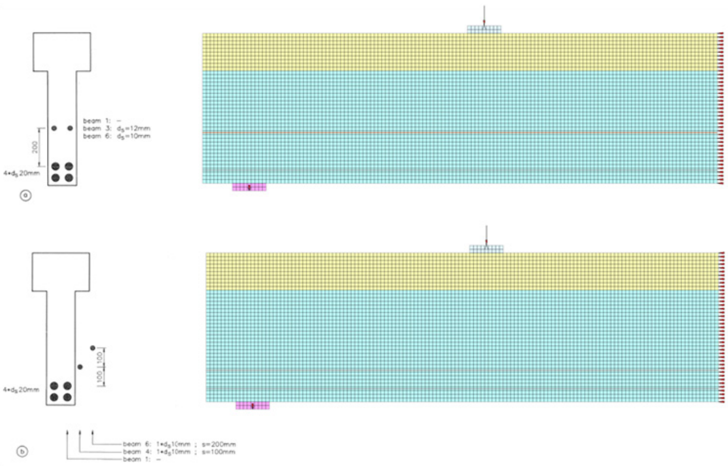

Figure 3. FE-mesh of half symmetric bending beam with force-load and supports

The material characteristics for the concrete are defined in the table 1. All parameters have been chosen such as defined in the reference, except the crack-energy parameter. The analysis has been done both crack-energy of 20 N/m and 100 N/m for both beams.

The material characteristics for the steel reinforcement bars are defined in table 2. These parameters have been chosen such as defined in the reference.

Young's modulus	28.9 GPa
Poison ratio	0.2
Density	3000 kg/m3
Tensile strength	3.82 MPa
Tensile softening curve	Hordyk
Crack Energy	20-100 N/m
Compressive Strength	61.7 MPa
Compressive failure curve	Thorenfeldt

Table 1. Material parameters for concrete Deep Beams

In a first load-step the full weight-load was applied and no cracking nor yielding occurred. Next a force-load of 50000 N was applied and the model still remained within the elastic regime. Finally, 490 increments of 500 N were applied and the maximum number of iterations was set to 25 iterations per load-increment. One analysis takes roughly 20 minutes on a modern PC.

Figures 4 and 5 show the force displacement-diagrams for Beam 1 and Beam 6, respectively for analysis with crack-energy of 20 N/m and 100 N/m and measurements reported in the reference report. These graphs show in general acceptable agreement between analysis results and measurement.

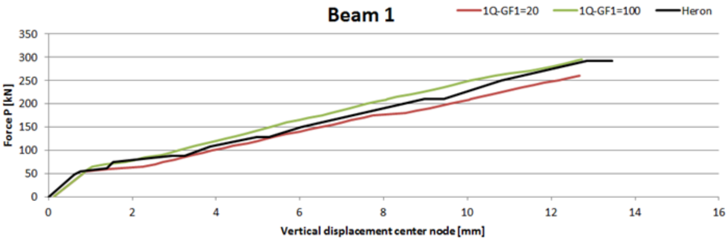

Figure 4: Force-displacement diagram for Beam 1 for different crack-energies, analysis results and measurements reported by C.R. Braam (Heron)

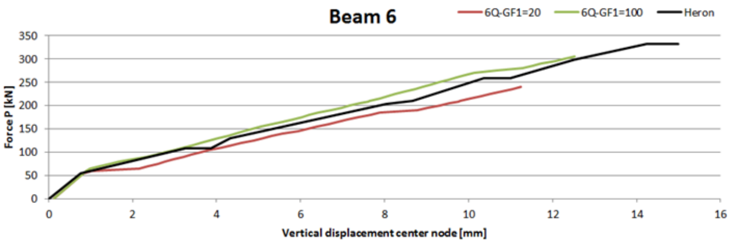

Figure 5: Force-displacement diagram for Beam 6 for different crack-energies, analysis results and measurements reported by C.R. Braam (Heron)

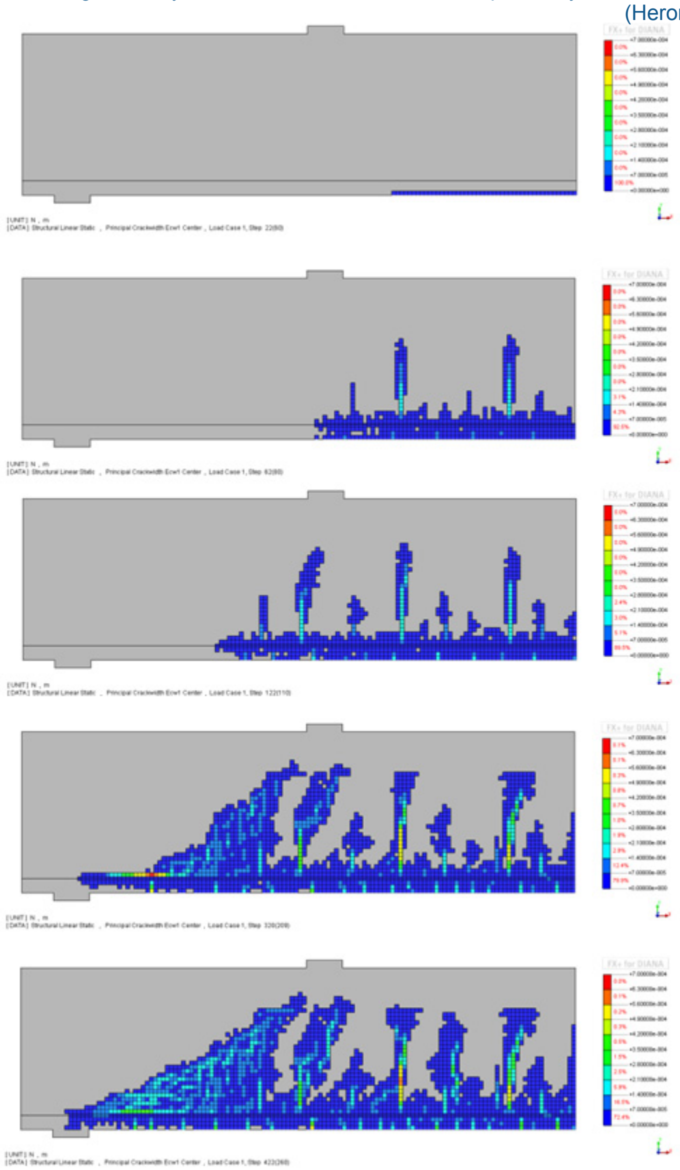

Figure 6: Crack-width at different load-levels (60, 85, 110, 209 and 240 kN) for model 1 with crack-energy of 100

Figure 6 and Figure 9 display the crack-width distribution for both beams with crack-energy of 100 N/m for different load-levels. For the purpose of these figures, the crack-width is defined as the product of the crack-bandwidth and the difference of maximum principal strain and maximum principal stress divided by the original Young's modulus. The crack-bandwidth was chosen equal to the length of one edge of the respective element. DIANA calculates the crack-bandwidth per element automatically. These figures illustrate the development of crack-patterns with increasing load-levels. In Beam 6, with extra reinforcement bar the crack-distance is smaller than for Beam1.

Calculated and measured crack distances are in agreement. The calculated local crack-widths are of the same order as the measured average crack-widths and variations of crack-width over height of the beam show also similar trends between analysis results and measurements.

Figures 7 and 10 display the stress in the reinforcement bars for both beams at a load of 209 kN. At this load-level the reinforcement stress is still below the yield-stress of steel. Stress concentration in the web-bar in Beam 6 can be clearly noticed.

Figures 8 and 11 display the reduction factor of the stiffness for both beams at a load-level of 209 kN. Crack-patterns can be clearly recognised but are not so strongly pronounced as in the crack-width results.

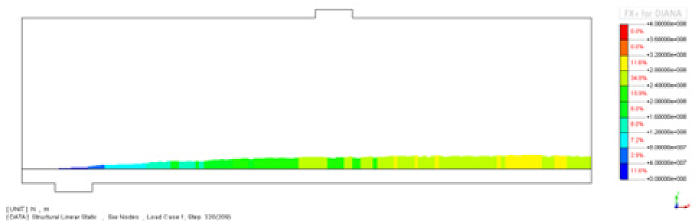

Figure 7: Stress in reinforcement bar for model 1 with crack-energy of 100 at load-level of 209 kN

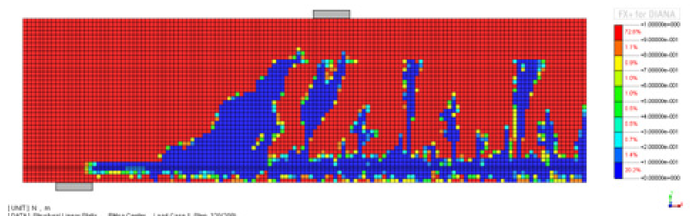

Figure 8: Stiffness reduction factor for model 1 with crack-energy of 100 at load-level of 209 kN

This example illustrates that Stiffness Adaptation Analysis can be used to predict crack-patterns and crack-width as well as deformations at serviceability loading levels in cross-sections of reinforced concrete beams. Analysis times are reasonable and analysis settings are straight-forward.

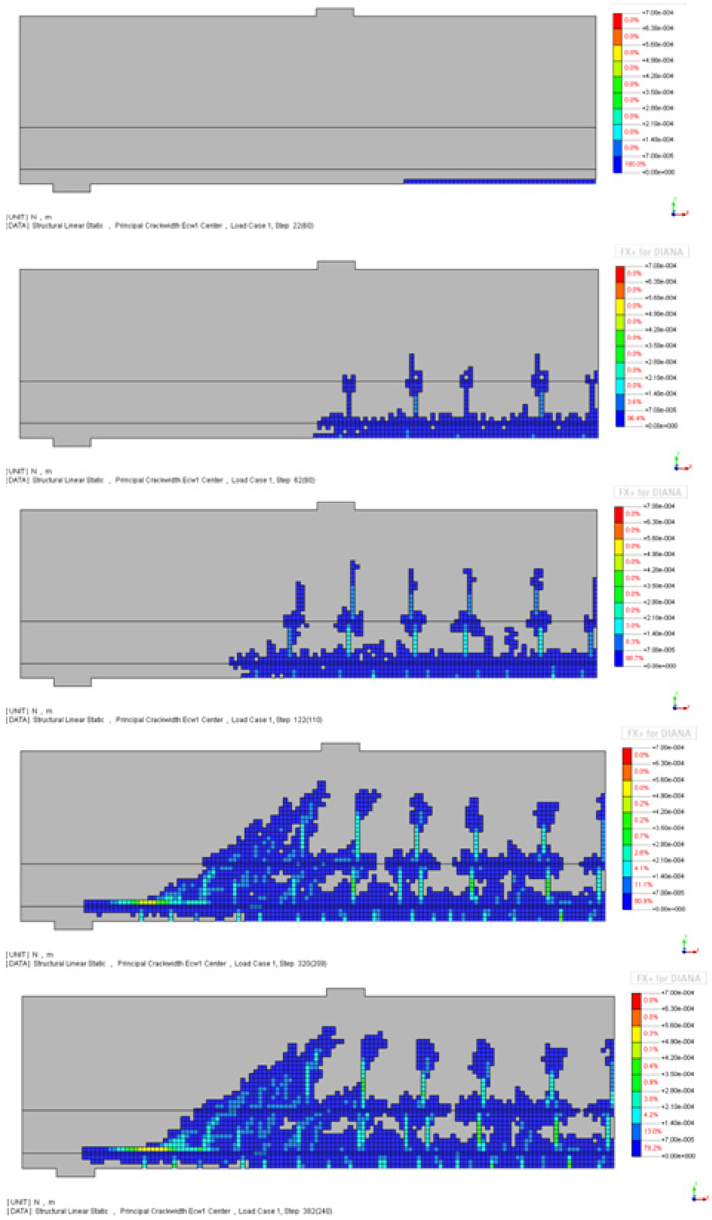

Figure 9: Crack-width at different load-levels (60, 85, 110, 209 and 240 kN) for model 6 with crack-energy of 100

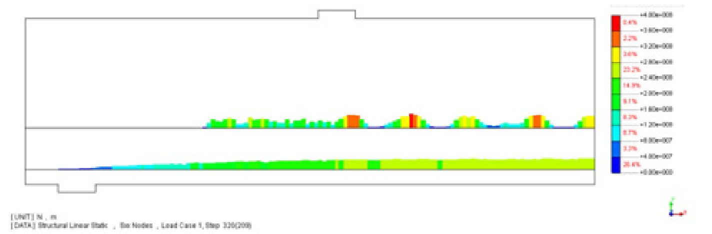

Figure 10: Stress in reinforcement bar for model 6 with crack-energy of 100 at load-level of 209 kN

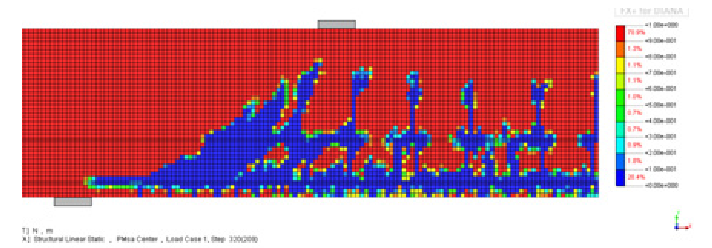

Figure 11: Stiffness reduction factor for model 6 with crack-energy of 100 at load-level of 209 kN

Flat Plate on Columns

The next analysis-example is a pre-stressed reinforced concrete floor on columns that is loaded by set-of point-loads.

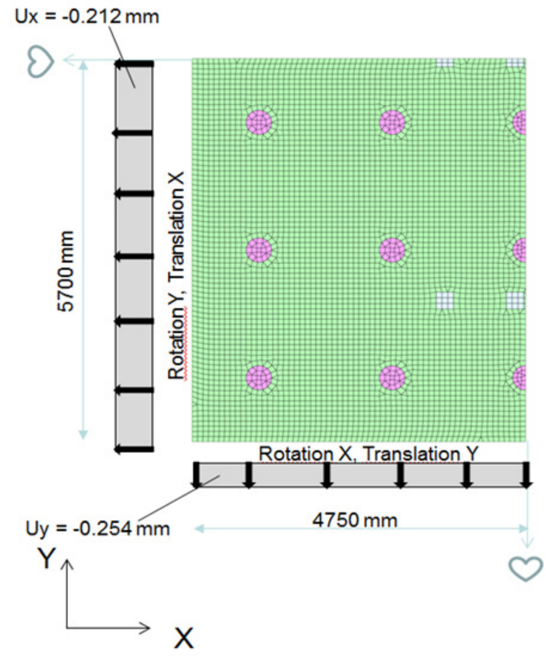

Figure 12: Mesh of Flat Plate on Columns with boundary conditions and elements

The floor is rectangular with dimensions 11400*9500 mm and is resting on 30 columns with diameter of 370 mm. For symmetry reasons only 1 quarter of the floor is modelled. In Figure 12 the positions of columns are coloured pink. The floor to column connection is modelled with linear interface elements. The 4 grey-coloured quadrilaterals in Figure 12 are the area's where a point-load-set is applied. The plate is modelled with quadratic shell elements with 7 integration-points over the thickness of the elements. The thickness of the plate is 190 mm and reinforcements grids of 0.503 mm at top side (bars 8 mm diameter and 100 mm spacing) and 0.424 mm at bottom side (9mm diameter and 150 mm spacing) In both directions are applied at both sides of the plate.

First a prescribed displacement is applied at the outer edges, to simulate the shrinkage of the flat plate. This shrinkage load corresponds with a tensile force of 361 kN/m. Next the weight-load is applied, followed by a distributed load of 10 kN/m2. Finally the point-loads are incremented.

The material characteristics for the concrete are defined in the table 3.

Young's modulus	28.9 GPa
Poisson ratio	0.2
Density	2500 kg/m3
Tensile strength	3.2 MPa
Tensile softening curve	Linear
Crack Energy	260 N/m
Compressive Strength	43 MPa
Compressive failure curve	Constant

Table 3: Material parameters for concrete of Flat Plate on Columns

And the material parameters for steel are defined in table 4.

Young's modulus	200 GPa
Poisson ratio	0.3
Yield Stress	500 MPa

Table 4: Material parameters for steel reinforcements in Flat Plate on Columns

Shrinkage, weight and distributed load are applied in subsequent steps, without any failure of materials. Next the point-set load is applied in 50 steps up to a total load of 270 kN. The analysis takes circa 5 hours.

Figure 13 displays the stiffness-reduction at the top-surface and at the bottom surface of the flat-plate. At the top-surface, cracking is initiated above the columns in diagonal direction, and with increasing loading, the cracks develop to arches around the areas where the sets of point-loads are applied. At the bottom surface, cracks are initiated in horizontal direction underneath the point-loads and with increasing loadings an additional vertical crack appears connecting the different sets of point-loads.

In Figure 14 the crack-width distribution at the bottom surface is shown. Crack-widths at the top-surface were small and therefore not displayed. In the bottom surface at 270 kN loading, the width of main cracks is up to 0.2 mm. At this load-level the reinforcement grids are still in the elastic regime.

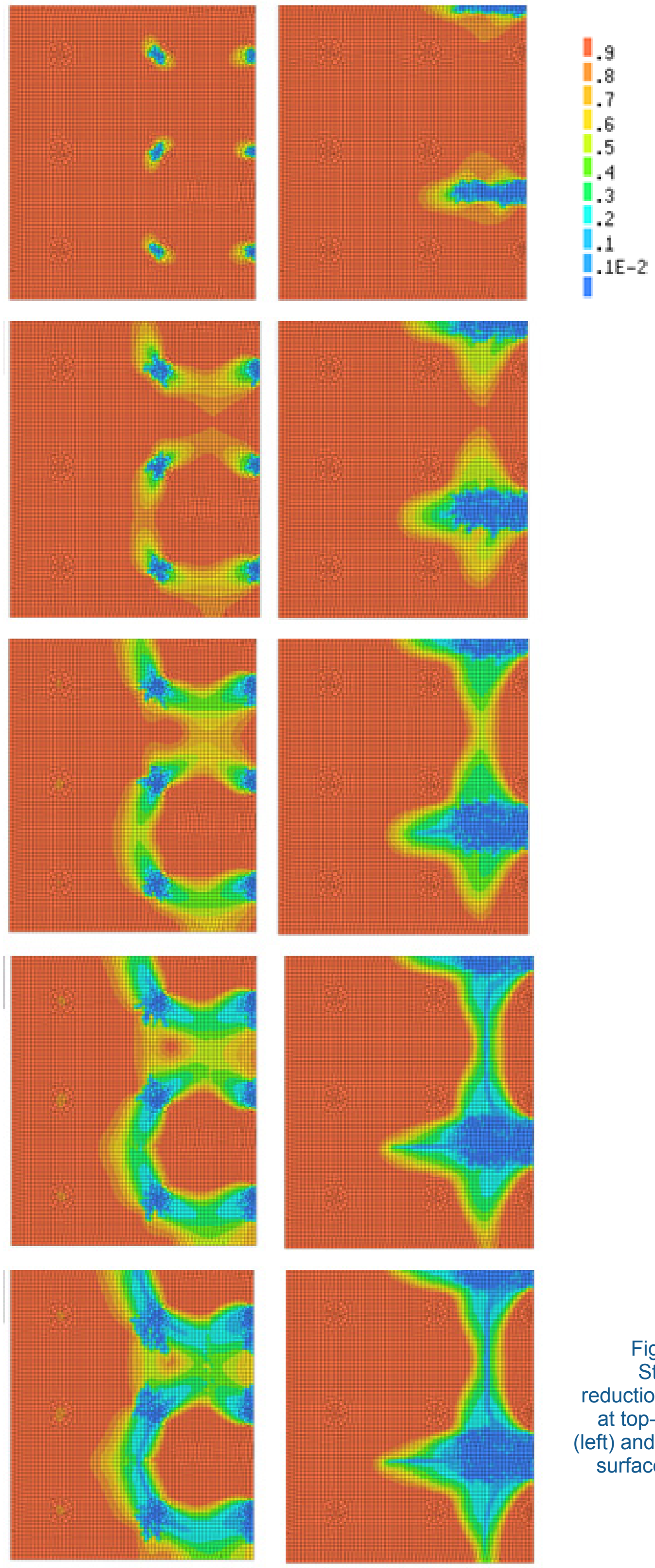

Figure 13: Stiffness-reduction factor at top-surface (left) and bottom surface (right)

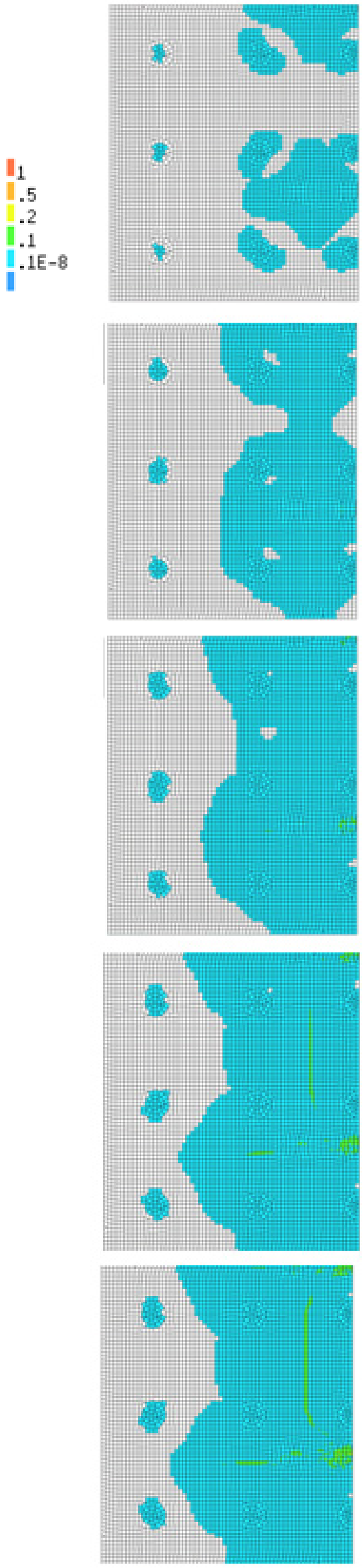

Figure 14: Crack-width distribution in mm at bottom surface

This example illustrates that Stiffness Adaptation Analysis can be used to predict crack-patterns and crack-width and onset of reinforcement yielding at serviceability loading levels in plate-type of structures. Analysis times are reasonable and analysis settings are straight-forward.

3D Masonry Structure

Full scale masonry structure tested by Yi et al. [2,3] is used as reference in the next analysis. In this experiment, a two-story unreinforced masonry structures, approximately 7.5 m square 7.1 m tall, was constructed and then tested under cyclic loading. For details of the experimental procedure, the reader is referred to [2,3]. De Jong et al. used the same reference for comparison with Sequential Linear Analysis and reported results in [4].

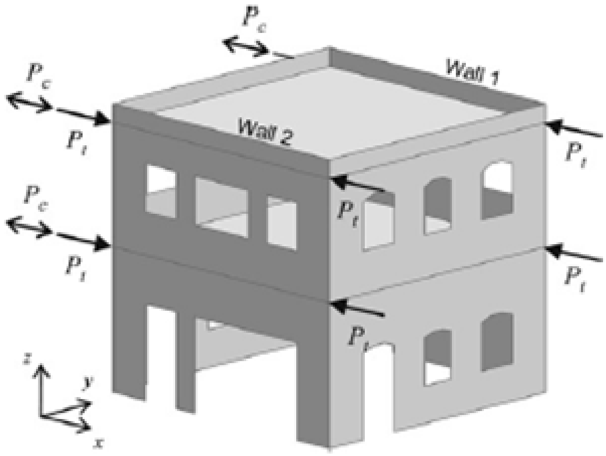

Figure 15: Geometry and loading conditions for model of Yi et al. [2] test

Figure 15 shows the outline of the building. First post-tensioning forces Pt were applied to the structures at 8 points, followed by a cyclic loading at the same locations as where the post-tensioning forces are acting. Cyclic loading was applied in displacement control, with the two equal floor displacements being fixed at 80% of the two equal roof displacements.

Prescribed displacements are always applied such that they lead to compressive reaction forces. Therefore, the supported degrees of freedom are different for both displacement directions. Because, Stiffness Adaptation Analysis in DIANA cannot at the moment be combined with Construction stage analysis, the cyclic loading experiments were simulated in two separate analyses by monotonic loading in the positive and negative x-direction. Results from both analyses were then combined to get an envelope for comparison with cyclic loading curves.

Young's modulus	6.9 GPa
Poisson ratio	0.25
Density	1920 kg/m3
Tensile strength	0.2 MPa
Tensile softening curve	Linear
Crack Energy	35 N/m
Compressive Strength	2 MPa
Compressive failure curve	Constant

Table 5: Material parameters for masonry elements in 3D Masonry structure

First, the weight load and the post-tensioning forces are applied in 1 step. Then the horizontal displacements were applied in 60 equal sized steps of 0.1 mm for the top-points. A maximum of 10 iterations for each load-step were defined.

The 3D building was defined with 4-node quadrilateral shell elements with 4 integration points in the plane and 3 integration points in thickness direction. Material properties for the masonry structures were defined as depicted in table 5. Thickness of the masonry was chosen equal to 250 mm.

The floor and roof are, as line-loads, acting to the walls with values equivalent to density of 450 kg/m3 and thickness of 200 mm.

Analysis time was circa 40 minutes per direction. Figure 16 depicts the measured cracks after full cyclic loading in both directions as reported by Yi et al. [4]. Figures 17 and 18 display crack-patterns, as reported by De Jong et al., for loading in + direction and in – direction, respectively. Figures 19 and 20 display crack-width results in the outer-surfaces of the walls at maximum loading (6 mm) for both loading directions.

The major crack wrapping from the top of the door-portal in Wall1 to the right-hand upper window in WallA can be recognised in Figure 16 and in both Sequential Linear Analysis and Stiffness Adaptation Analysis results with loading in + direction (Figures 18 and 20). A major crack starting at the footing of the door-portal in Wall1 and wrapping to the left-hand upper window in WallB can be recognised in both analysis results for loading in – direction, but not in the Figure 16. As De Jong [5] writes, this discrepancy is likely to be the result of simplified monotonic loading.

Figures 21 and 22 show the displacement reaction force curves as measured by Li et al. [4] and as calculated by Stiffness Adaptation Analysis for Wall 1 and Wall2 respectively. Both results show good agreement in initial stiffness and reasonable agreement in maximum shear-force capacity.

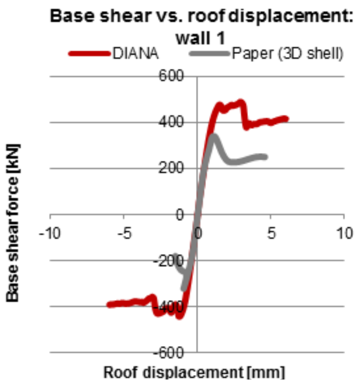

Figure 21: Base shear versus roof-displacements for wall 1

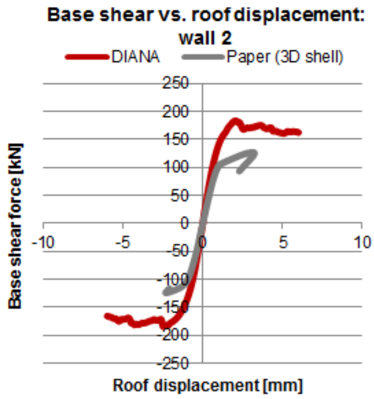

Figure 21: Base shear versus roof-displacements for wall 2

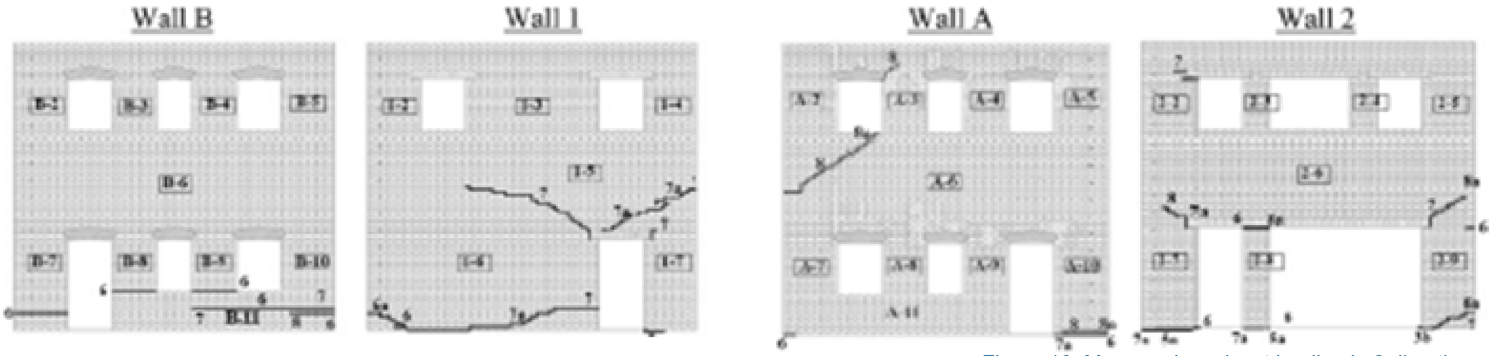

Figure 16: Measured cracks at loading in 2 directions

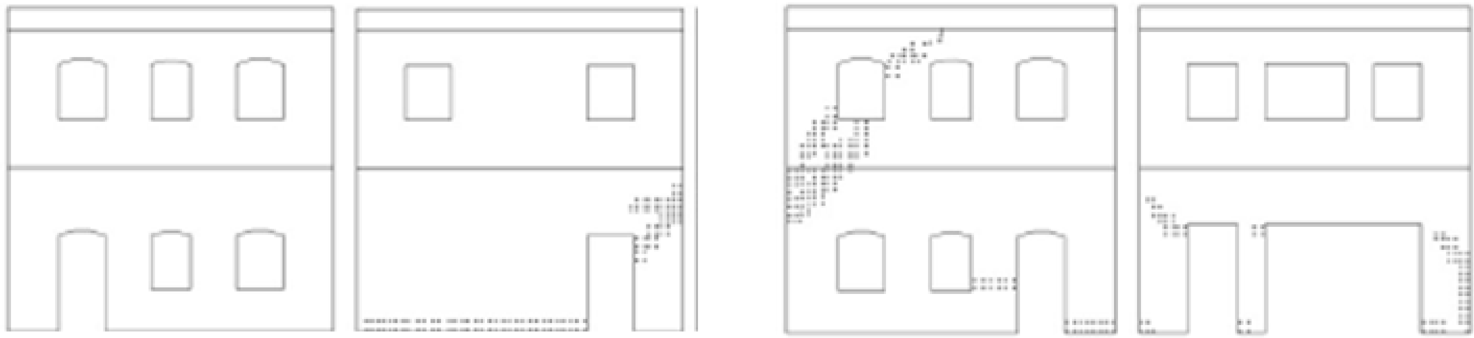
Figure 17: Cracks as results from Sequential Linear Analysis reported by de Jong et al. in [5] in + loading direction

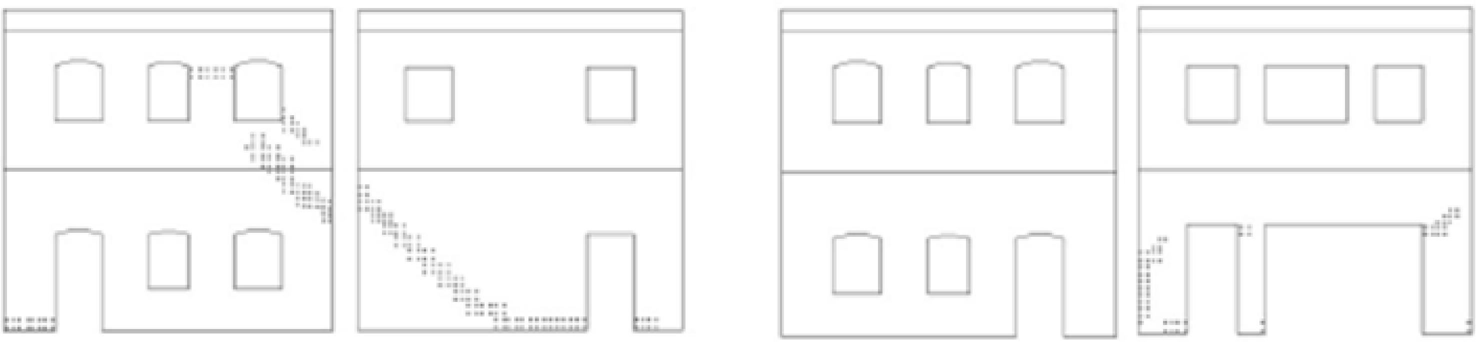
Figure 18: Cracks as results from Sequential Linear Analysis reported by de Jong et al. in [5] in - loading direction

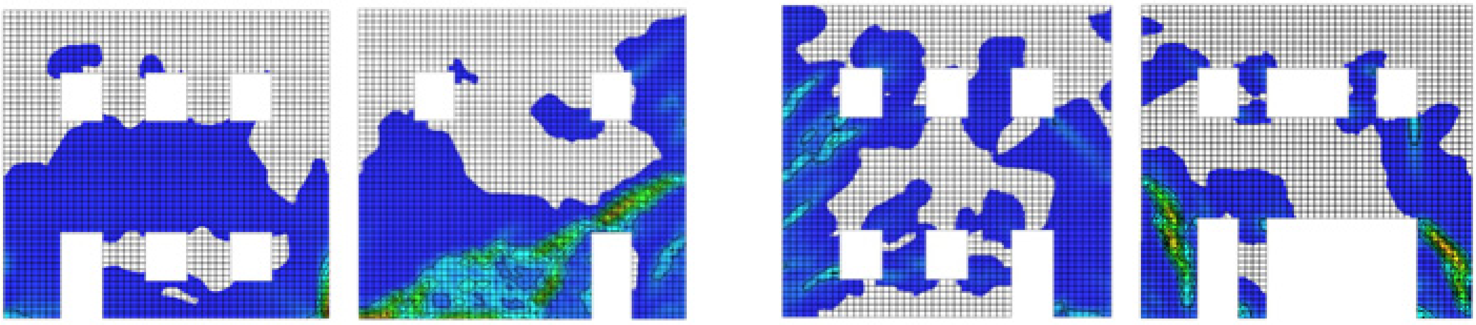
Figure 19: Cracks as result from Stiffness Adaptation Analysis in + loading direction at 6mm prescribed displacements

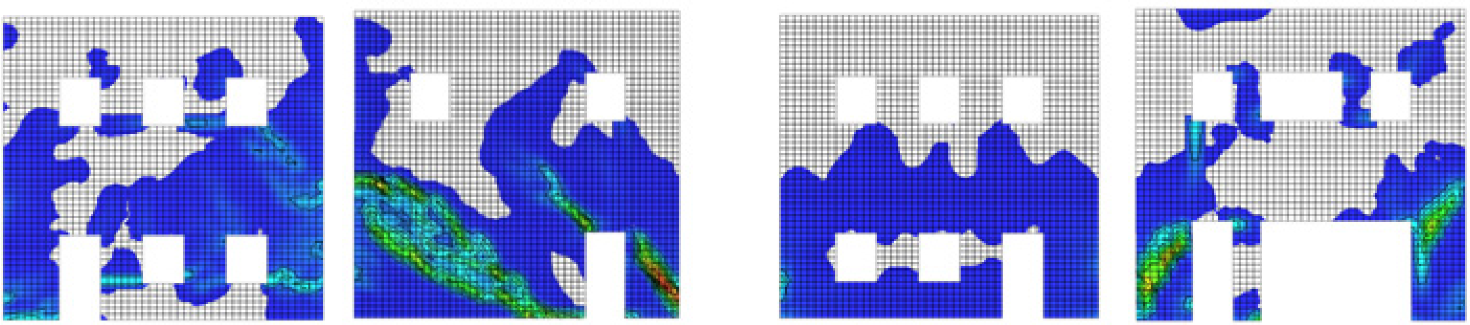
Figure 20: Cracks as results from Stiffness Adaptation Analysis in + loading direction at 6mm prescribed displacements

3D Viaduct

One 60 meters segment of a single span out of a 15 spandouble-box-girder viaduct (986 m length in total) is used as basis for the last example of this paper. In the bridge segment an expansion-joint is defined and both parts are connected with a rigid dowel. Cracks in the concrete body were noticed during inspection and analyses have been performed to assess crack development and the stability of the bridge at load-levels between serviceability and ultimate limit state.

A 3-dimensional finite element model of solid elements was defined for the concrete body, taking into account construction details, such as variations of thickness of flanges and walls of the box, man-hole-openings and anchor-bolts. The finite element models consists of circa 82.000 lower order elements, mainly of brick-type.

A series of pre-tensioning cables is defined in each of the walls of the boxes. A very detailed representation of the steel reinforcements in the box-girder was considered, such as longitudinal bars in the box, transverse bars in the top-flange, curved pre-tension cables in the end-plates, grids at all outer faces of the concrete body, and others. The total number of reinforcement particles in this model is around 310.000.

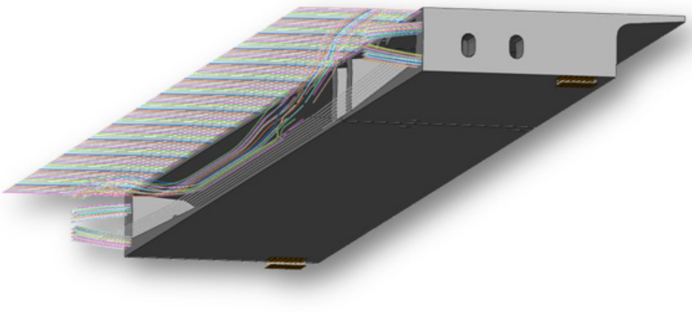

Figure 23: Part of the concrete body of the box-girder viaduct with selected of reinforcements in the structure

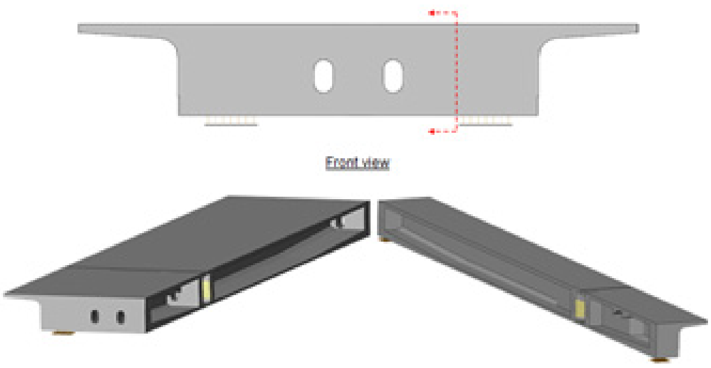

Figure 24: Front view of box-girder viaduct with splitted view

Concrete was defined with linear softening in tension and constant maximum stress in compression. Steel reinforcements were defined with constant maximum stress in both tension and compression.

Both parts were connected with rigid interface elements in the joint. The viaduct was supported in 4 corner points on elastic interface elements. Further, all the nodes in the longitudinal end-planes are supported in axial direction. The load was applied as follows:

- First the weight-load and pre-stressing of the longitudinal cables in the walls of the box were applied in 10 increments.
- Then the P-mobile load was applied in 10 increments. The P-load is positioned as 6 rectangular pressure field eccentrically on the shorter part of the model close to the joint. P-load is defined according Eurocode.
- Then the Q-mobile load in 30 increments of 10% each. The Q-mobile load is defined as pressure load on the full top-surface of the segment and is defined according to Eurocode.

No construction stages have been considered.

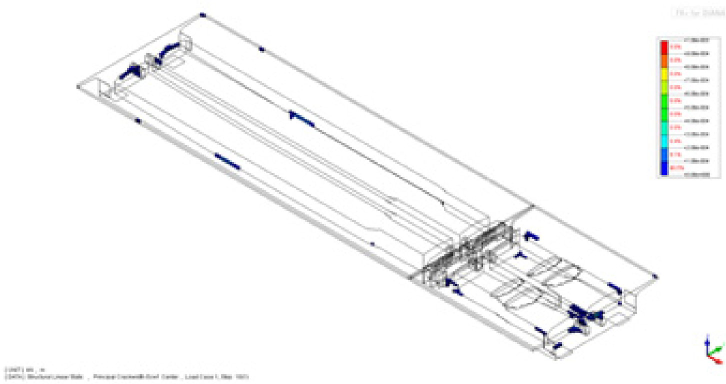

Figure 25: Crack pattern with crack-widths after weight load and pre-tensioning load

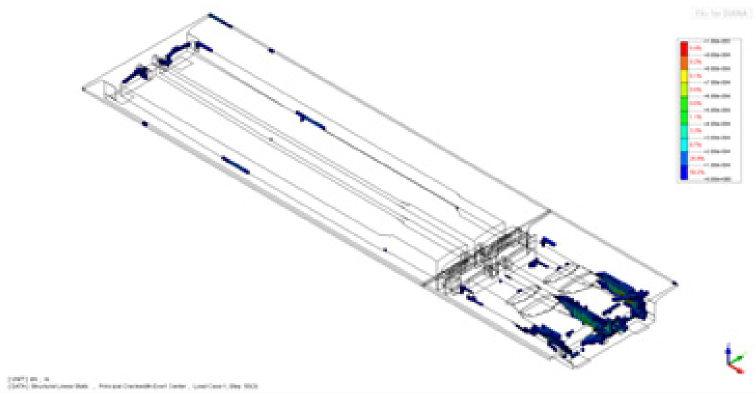

Figure 26: Crack pattern with crack-widths after weight load and pre-tensioning load, 1x P-Mobile and 3x Q-mobile (from top-right direction)

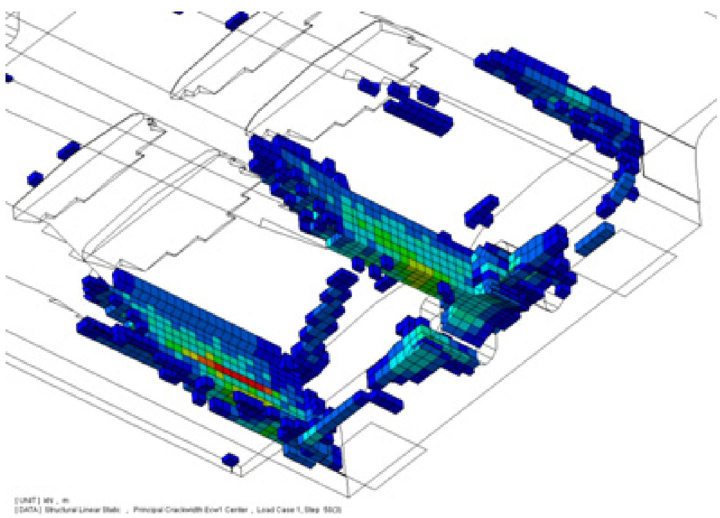

Figure 27: Crack pattern with crack-widths after weight load and pre-tensioning load, 1x P-mobile and 3x Q-mobile (detail from bottom left direction).

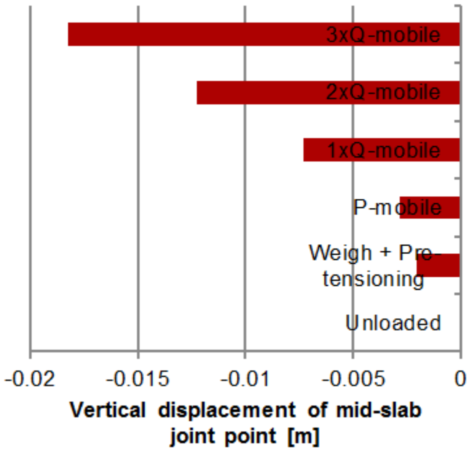

Figure 28: Vertical displacement of position next to the joint at mid-point of top-deck

A stiffness-adaptation analysis has been performed on a dual Intel® Xeon® X5550 quad-core 2.66GHz, 48 GB memory, Linux platform with elapsed time of 10 hours.

Figures 25 and 26 display crack-patterns and crack-widths in the box-girder after application of weight and pre-tensioning loading (Figure 25) and after application of 3xQ-mobile (Figure 26). After initial loading the maximum crack-width is limited to 0.1 mm and small cracks are found locally at transitions from the top and the bottom flange and the walls of the box-girder. When the full loading (3x Q-mobile) is applied severe horizontal, slightly diagonal, cracks are found in the walls of the shorter part of the viaduct segment. Crack-width in the wall at the side of the bridge at which P-mobile is applied is of order of 1 mm whereas in the middle wall of the box-girder the

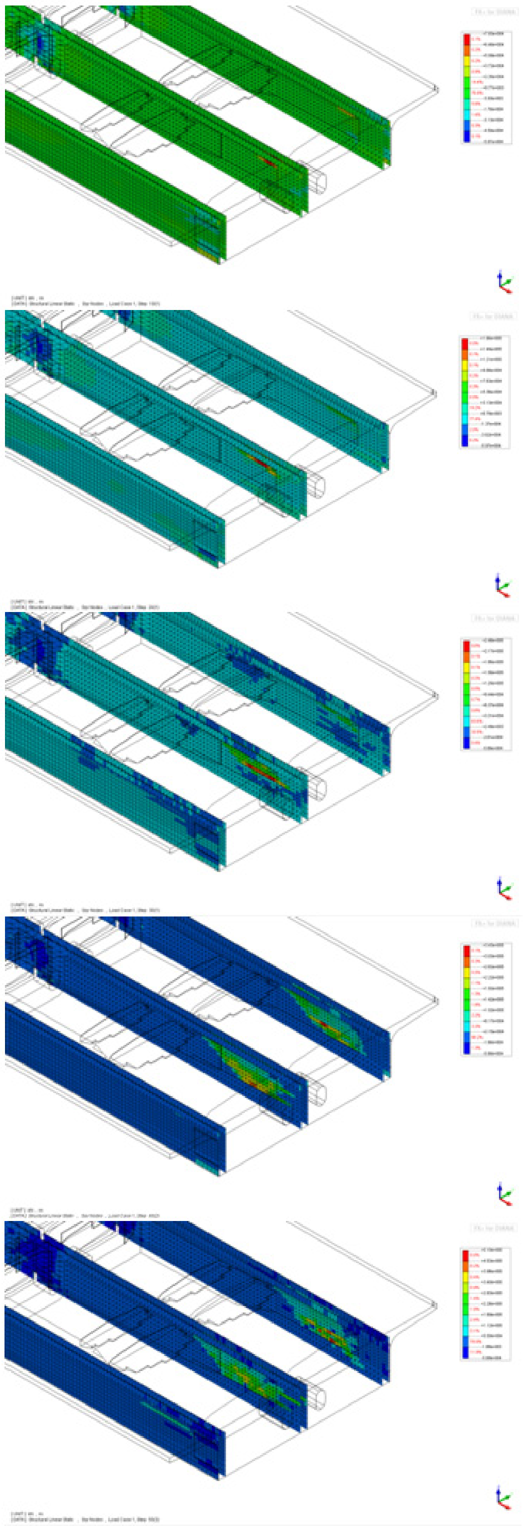

Figure 29: Vertical stresses in reinforcement grid walls...

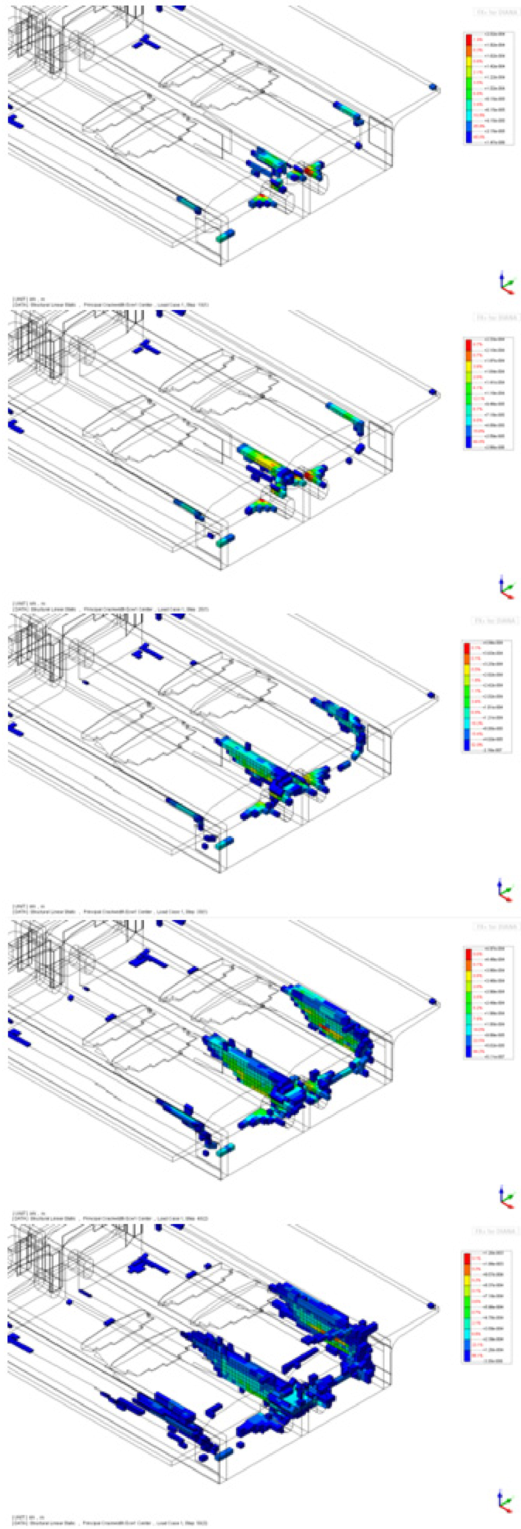

... and crack-widths at different load levels crack-width are limited to 0.4 mm in the mid-span and 0.2 mm in the right-hand-side span). Figure 27 shows that at 3x Q-mobile loading a diagonal crack propagates through the upper-flange initiating at the corner connection of top-flange, end-plate and left-hand-side wall.

Figure 28 shows the development of vertical displacements of a node positioned in the middle of the top-flange close to the joint as function of 5 loading conditions. With the progressing of cracks the displacement develops progressively in the three last bars with constant increase of loads.

The figure 29 shows a selection of stresses in reinforcement grids with corresponding crack-patterns in the shorter part of the box-girder box.

References

[1] HERON Nr. 35, 1990, *C.R. Braam, Control of Crack-width in Deep Reinforced Concrete Beams*

[2] Yi T., *Large-scale testing of a two-story URM structure, Ph.D. dissertation Georgia Institute of Technology, 2004.*

[3] Yi T., Moon F.L., Leon R.T., Kahn L.F., *Lateral load tests on a two-story unreinforced masonry building, ASCE J. Struct. Eng 2006: 132(5):643-52.*

[4] De Jong M.J., Belletti, B., Hendriks M.A.N., Rots, J.G., *Shell elements for sequential linear analysis: Lateral failure of masonry structures, Engng. Structures 31 (2009) 1382-1392.*

5th International Seminar: Advanced Analysis of Bridges & Structures

The above paper (" The Prediction of Crack-width and Crack-patterns"), was just one of the papers presented at this year's International Seminar which was held on the 23rd November at the Institution of Structural Engineers in London.

TNO DIANA BV was joined by around 50 participants with varying levels of experience from various areas of the Civil Engineering practice, all with a keen interest in the development of applications of advanced analysis in engineering practice.

In addition to the above, interesting and informative presentations were given by our colleagues at:

- Gifford Advanced Engineering
- Hewson Consulting Engineers
- Arup Advanced Technology Group
- Royal Haskoning
- Ingenieria Zero
- Universitat Politecnica de Catalunya (Barcelona Tech)
- Imperial College

Gerd-Jan Schreppers, TNO DIANA BV
"The Prediction of Crack-width & Crack-patterns"

Jose Turmo, Barcelona Tech
"Construction of Concrete Structures with Externally Unbonded Tendons"

Numerical Analysis for Nonlinear Seismic Tunnel-Soil Interaction Analysis

Author: P. Chatterjee,
TNO DIANA BV

The objective of the present study is to develop a three-dimensional (3D) numerical model in DIANA for performing nonlinear tunnel-soil interaction analysis when the system is subjected to the action of a unilateral ground motion. In order to perform the seismic soil-tunnel interaction analysis, the free vibration analysis of the whole model is first carried out to identify the mode shapes and the dominant frequencies and modal mass participation factors. These would also enable to ascertain the values of Rayleigh damping parameters. Thereafter, the response spectrum analysis corresponding to a design response spectrum has been performed followed by a time history analysis assuming the nonlinear tunnel-soil system being subjected to a specific ground motion corresponding to Loma Prieta earthquake (1988).

Figure 1 shows the tunnel embedded in the soil domain. The soil is made up of hard rock type of material. The tunnel consists of 2 parts – one is the main tunnel running through the soil along Y-Y direction and the other part is the gallery which has a short extension along X-X direction to and gets connected to the main tunnel. The main tunnel and the gallery are made up of concrete (shotcrete). The tunnel parts are connected to the soil through rock bolts. The material properties of the soil, the tunnel and the rock bolts are given in Table 1 below.

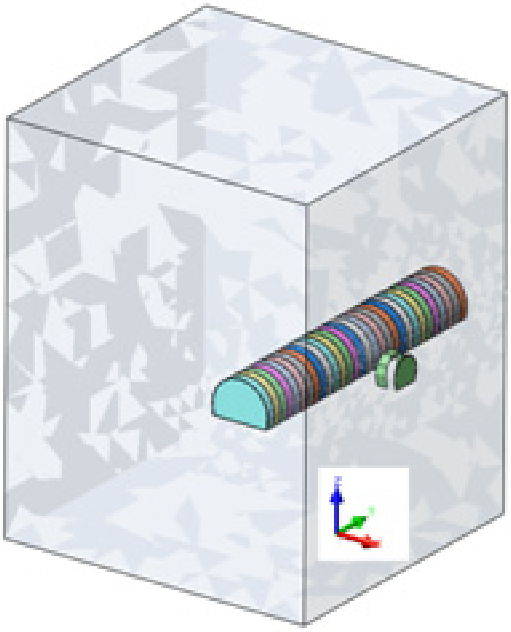

Figure 1: Tunnel-soil model

The soil has been meshed with tetrahedral solid elements and the tunnel mesh consists of curved shell elements of uniform thickness 0.16 m. The rock bolts composed of 1-dimensional reinforced bar elements of uniform cross-section area 0.000491 m2 (which corresponds to a diameter of 25 mm). The dimensions of the soil block considered for the analysis are 64 m (=dX) by 60 m (=dY) by 80 m (=dZ). The tunnel length is 60 m.

Parameter	Unit	Soil	Tunnel	Rock Bolt
Model Type	-	Mohr-Coulomb	Elastic	Elastic
Elastic Modulus	kN/m^2	5883990	14709975	196133000
Mass Density	kN/m^3	25.49	23.57	76.96
Poisson's Ratio	-	0.2	0.2	0.3
Cohesion	kN/m^2	2941.995	-	-
Friction Angle	0	40	-	-
Dilatancy Angle	0	0	-	-

Table 1

The model is fixed against translations in all directions at the bottom. The lateral faces on global XZ plane are fixed against motion in Y direction and the lateral faces in YZ plane are restrained against motion in X direction. The two extreme ends of the main tunnel are also fixed against rotations about global X and Z axes. Beside the self-weight, seismic motion is applied in the model in form of base excitation only along the horizontal X axis. The model is first analysed to establish the dominant eigen frequencies corresponding to the free vibration. The eigen analysis reveals 6th and 8th modes with frequencies 11.83 Hz and 12.74 Hz respectively being important for translation vibration in X direction, 7th and 10th modes at 12.32 Hz and 13.44 Hz respectively to be determining for vibrations in Y direction and 1st and 13th modes at 4.96 Hz and 14.96 Hz respectively to be the most influential modes for the vertical vibration of the tunnel-soil system. The frequencies are high because of the stiff nature of the system considered. Figure 2 shows the normalised deformation pattern corresponding to mode 6 (in horizontal (X) direction) and mode 10 (in horizontal (Y) direction).

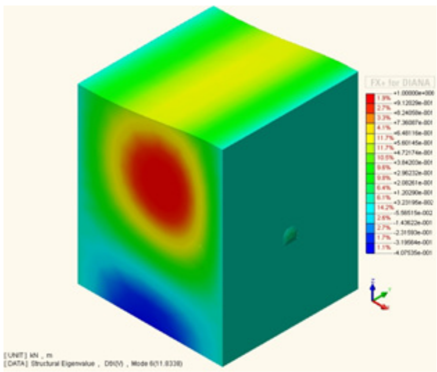

Figure 2: Mode shapes of the model corresponding to mode 6 in X-direction (above) and mode 10 in Y-direction (right)

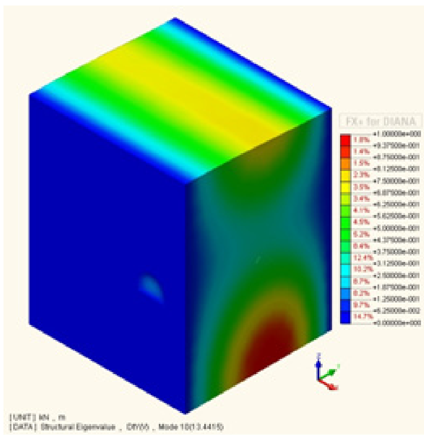

Subsequently, a response spectrum analysis has been performed with an input of a design response spectrum (applied in horizontal X direction) as shown in Figure 3. The eigen frequencies were observed to be distinctly spaced. Hence, the square root of sum of squares (SRSS) method of modal combination rule has been adopted for superposition of results for the first 15 eigen frequencies. The soil is assumed to have a damping ratio (ζ) of 5%. From the eigen analysis the dominant eigen frequencies (ωn) have been spotted to be within a range of 4 Hz and 15 Hz. For this range with 5% damping, the Rayleigh damping parameters (α and β) may be obtained from the following equation.

$$2\zeta\omega_n=\alpha+\beta\omega_n^2 \quad (1)$$

The Rayleigh damping parameters, thus, may be computed as 1.98496 (α) and 0.0008373 (β).

These values are also now included in the material parameter definition of the numerical model. The horizontal normal stresses (in X direction) in the 3D soil elements and the 2D tunnel elements obtained from the response spectrum analysis are shown in Figure 4. These values correspond to the absolute peak values of the response which may practically occur at different time instants. It may be mentioned here that the red and blue colours correspond to maximum and minimum values of the response respectively. The maximum values of the stress field reach 29.56 kN/m2 and 50.70 kN/m2 in cases of soil and tunnel respectively whereas the minimum stress values for the soil and the tunnel are respectively 1.19 kN/m2 and 0.21 kN/m2. Figure 4 reveals that the stresses in the soil are more on the boundaries. The connecting gallery is subjected to higher stresses than the main tunnel.

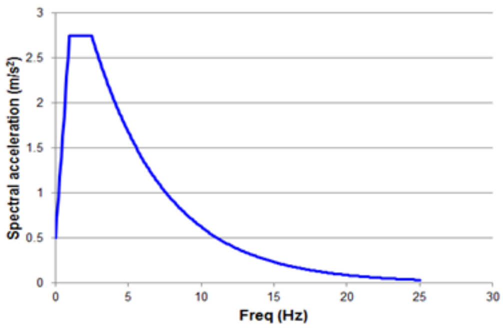

Figure 3: Design response spectrum load

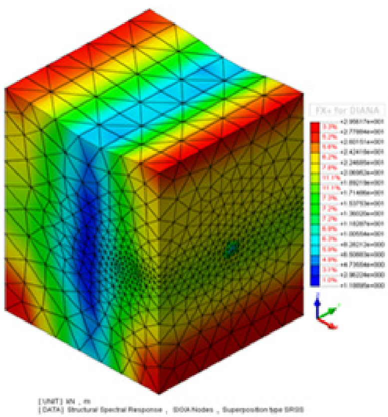

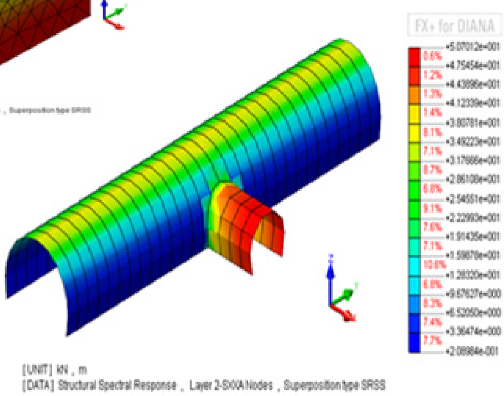

Figure 4: Horizontal (X) normal stresses in soil (above) and tunnel (right)

The same model is now subjected to a horizontal (X direction) seismic base excitation in the form of a time history (of acceleration) loading as shown in Figure 5. This accelerogram corresponds to Loma Prieta ground motion (1988) at Dumbarton bridge site and spans over a duration of 39.98 s. The nonlinear time history analysis is performed in DIANA. The Newmark time integration scheme has been chosen with values of integration parameters β=0.25 and γ=0.5. The consistent mass matrix and consistent damping matrix have been considered. The first step in the calculation involves stress initialization and obtaining equilibrium of stress state due to self-weight. Next, the time history analysis has been performed over the model for the whole duration. The time increment is chosen as 0.02 s. The temporal variation of displacements responses resulting at specific nodes at the bottom of the tunnel and the top surface of the soil domain (directly above the tunnel) are shown in Figures 6 and 7 respectively. These are the relative displacements with respect to the displacements at the bottom line of the model. Figure 7 clearly demonstrates that the motion is amplified at the ground surface which is having higher values of peak displacements compared to the displacements due to tunnel vibration as seen in Figure 6.

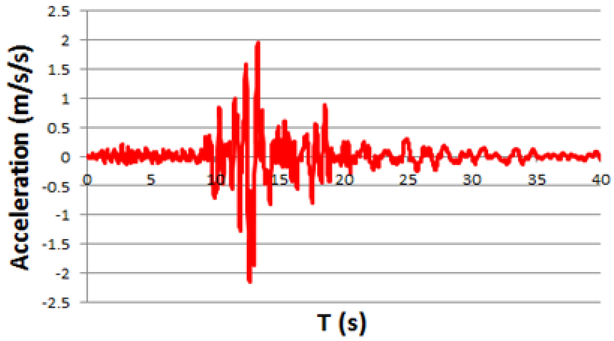

Figure 5: Horizontal base excitation (Loma Prieta. 1988)

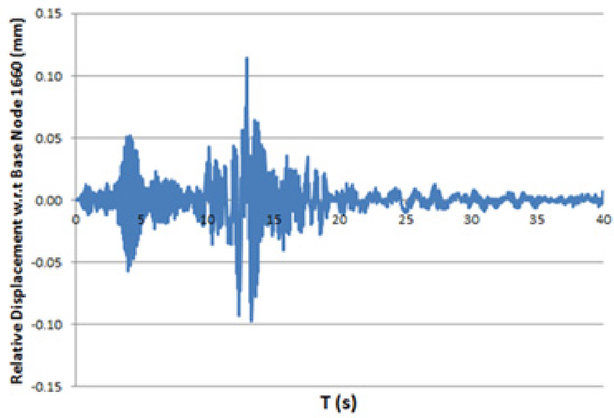

Figure 6: Displacement time history at tunnel (main) bottom

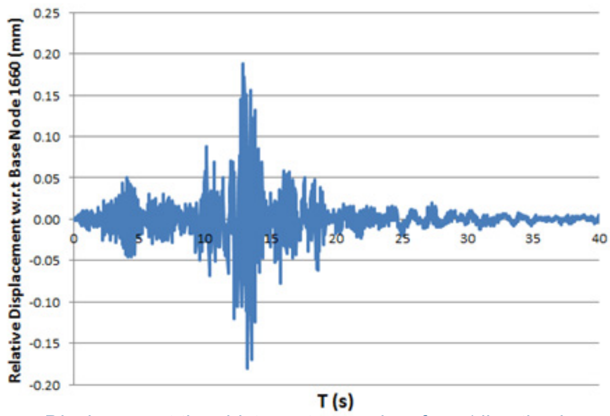

Figure 7: Displacement time history at ground surface (directly above the tunnel)

Concrack 2: Control of cracking in R.C. structures: results obtained with DIANA for the test case SHW

Authors: Cecilia Damoni &
Beatrice Belletti,
University of Parma, Italy
Giovanna Lilliu, TNO DIANA BV,
The Netherlands

Introduction

In the current paper the results obtained from nonlinear finite element analyses for a squat shear wall, denoted as test case SHW, subjected to monotonic shear loading are discussed. Numerical results are compared with experimental results driven from CEOS.fr, dealing with the modeling of the behavior of the mocks-ups tested (monotonic and cycling loading-prevented or free shrinkage). The analyses are performed with the finite element code DIANA 9.3 [1]. In the following sections the model used is described and some of the main parameters that influence nonlinear finite element analyses results, regarding for instance the crack model adopted, are further investigated in order to deepen the structural assessment obtained.

Experimental set-up and mechanical properties

The squat shear wall tested in laboratory is clamped at the top and at the bottom in two highly reinforced beams and the left and right extremities are seamed with rebars. The wall is placed in a rigid metallic frame and subjected to monotonic loading-unloading through two jacks placed at the top of the wall. Experimental sensors are placed on the two faces of the wall in order to measure the crack opening and the strain in rebars. In Fig. 1 the experimental bench is illustrated and in Table 1 the main material mechanical properties are reported. In Fig. 2 the dimensions of the wall with the reinforcement layout are plotted. The total height of the wall is 2470 mm, the total length is 4700 mm and the main reinforcement grid, placed in the web panel, is constituted of □10/10mm. For further geometrical details please refer to [2] and [3].

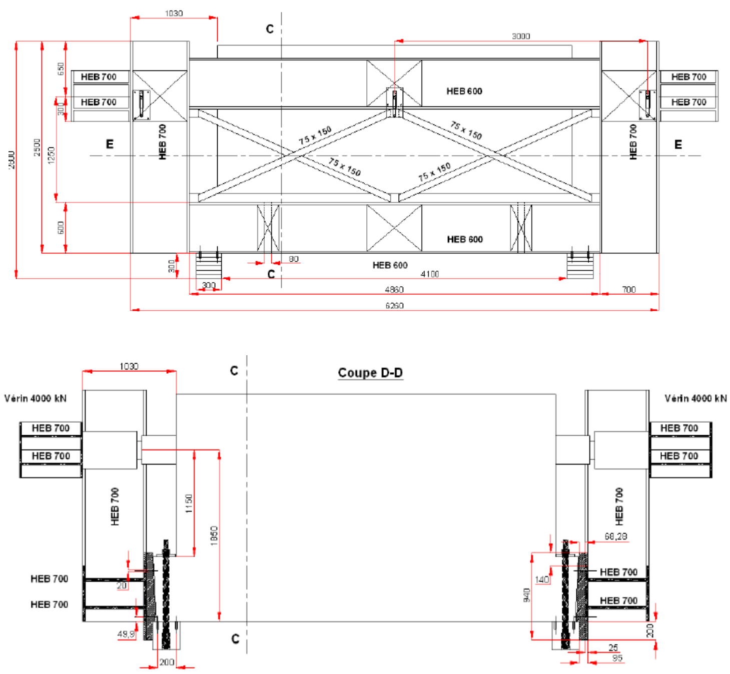

Figure 1. Experimental bench

Concrete		Steel	
f_c (MPa)	-42.5	f_y (MPa)	554
f_t (MPa)	3.3	E_s (MPa)	189274
E_c (MPa)	22060	f_u (MPa)	634

Table 1. Material mechanical properties

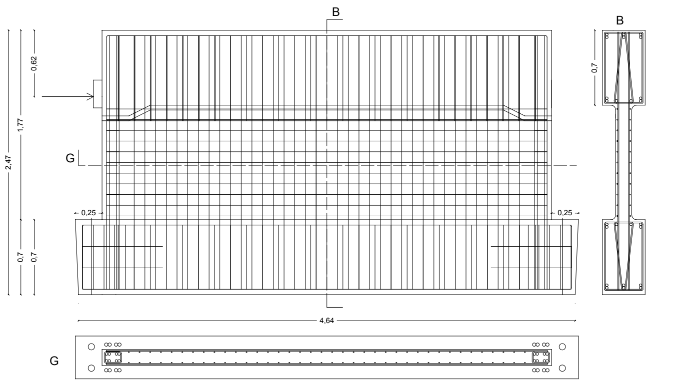

Figure 2. Reinforcement layout

Modelling of the squat shear wall

A 2D modeling is adopted to simulate the test. A loading steel plate is introduced to apply the monotonic shear loading and interface elements are inserted between the loading plate and the concrete elements. The concrete elements, with an average dimension of 100mm x 100mm, and the loading plate are modeled through eight-node quadrilateral isoparametric plane stress elements based on quadratic interpolation and 3x3 Gauss integration. For the reinforcement embedded truss elements are adopted. In a first simplified modeling all the nodes of the lower flange are restraint along “y” direction and the nodes seamed with rebars in the built test along “x” direction. Regarding the crack model used, a total strain fixed crack model is adopted. To model the concrete behavior a parabolic law in compression, based on the definition of a compressive fracture energy, and an exponential law in tension are used; the reduction of the compressive strength due to lateral cracking is taken into account in the mechanical model. For the reinforcement an elasto-plastic with hardening model is adopted. The analyses are performed in displacement control, calibrating the displacement applied at each step in order to reach the load value imposed in the test. A standard Newton-Raphson convergence method is adopted with a maximum number of 25 iteration per step and a combination of energy based convergence criterion with a tolerance of 10-3 and force based convergence criterion with a tolerance of 10-2 are applied.

In Fig. 3 the mesh adopted with indication of boundary conditions and material constitutive model is plotted.

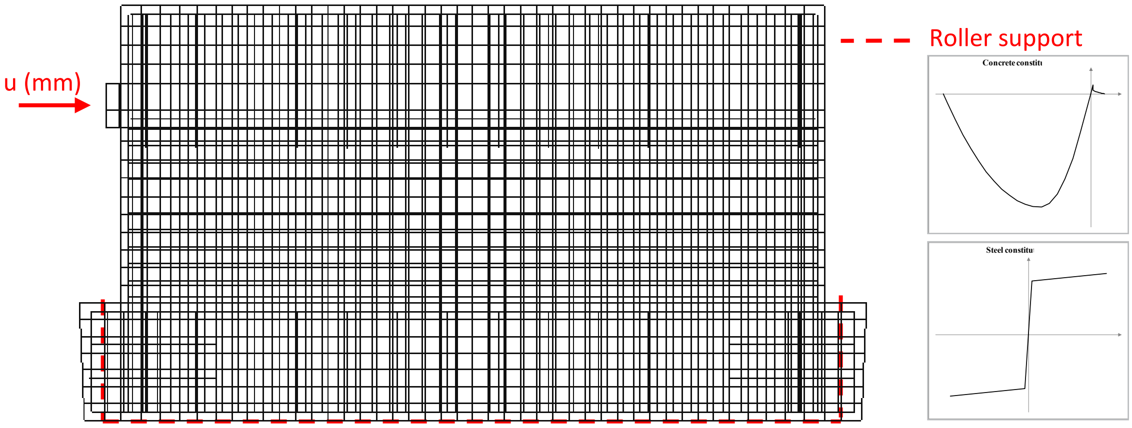

Figure 3. Mesh adopted

Results

According to the results obtained with DIANA 9.3 the shear wall subjected to monotonic loading-unloading fails in shear due to crushing of concrete, as observed in the experiment. The cracks start to develop from the low left side of the web and spread through the entire web until the right side of the web, with concrete struts inclination of about 45°. The highest concentration of cracks is placed under the loading plate on the top left side of the web and in the low right side of the web. In these positions the concrete completely crushes. None of the reinforcing bars reach yielding.

As already mentioned in section 3 a total strain fixed crack model is used to perform the analyses: the software used applies a constant shear retention factor, chosen for the first simulation equal to 0.1. The reduction of the compressive strength due to lateral cracking, allowed in the model, follows the “Model B” proposed by Vecchio & Collins [4]. Fig. 4(a) shows the load-displacement curves obtained from nonlinear finite element analyses in which the tension stiffening effect is neglected or is taken into account by increasing the ultimate cracking strain up to the reinforcement yielding strain value. It can be noted the big influence of the tension stiffening effect especially on the ultimate load reached. Also the crack pattern obtained, much more spread and uniform respect the case in which the tension stiffening effect is neglected, is more similar to the experimental one. In Fig. 4(b) the maximum principal strain obtained from the numerical simulation are compared to the experimental crack pattern; the minimum principal strain, indicative of the crushing of concrete, are also reported.

It is important to note that in the current model implemented in the software used the behavior in loading and unloading is modeled through secant unloading, so that residual plastic strain are not evaluated.

As already previously mentioned, regarding the fixed crack model used, the current model implemented in the software considers a constant shear retention factor to be inputted in the analyses; in this way the aggregate interlock effect is not properly taken into account and the results obtained can be affected by the shear retention factor value chosen. In Fig. 5(a) the effect of shear retention factor, chosen equal to 0.1 and 0.5, are reported.

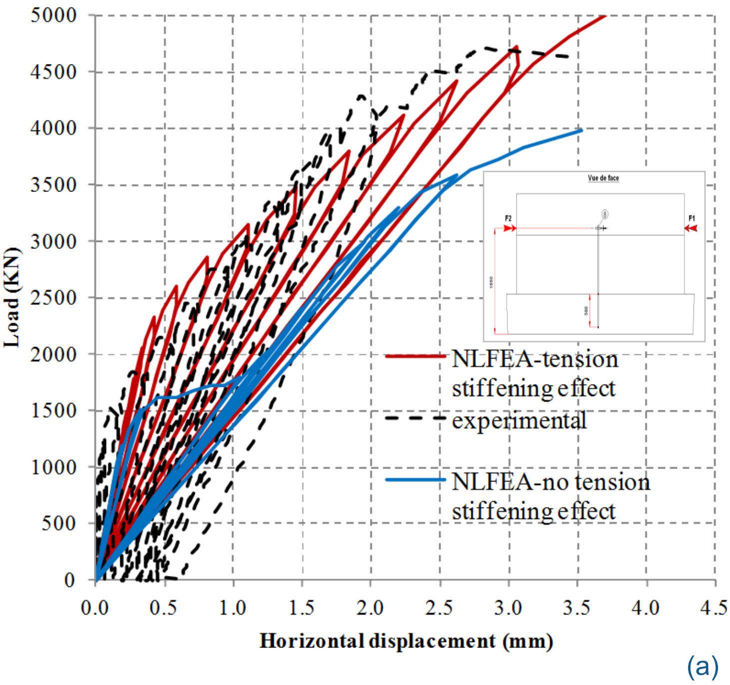

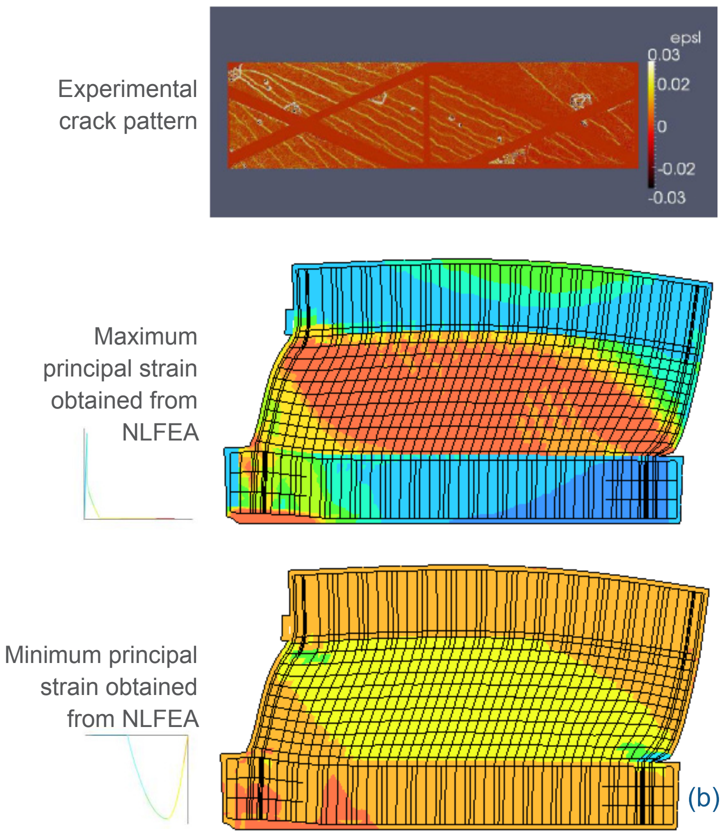

Figure 4. (a) Load-displacement curves, (b) experimental crack pattern and maximum and minimum principal strain obtained from the numerical model

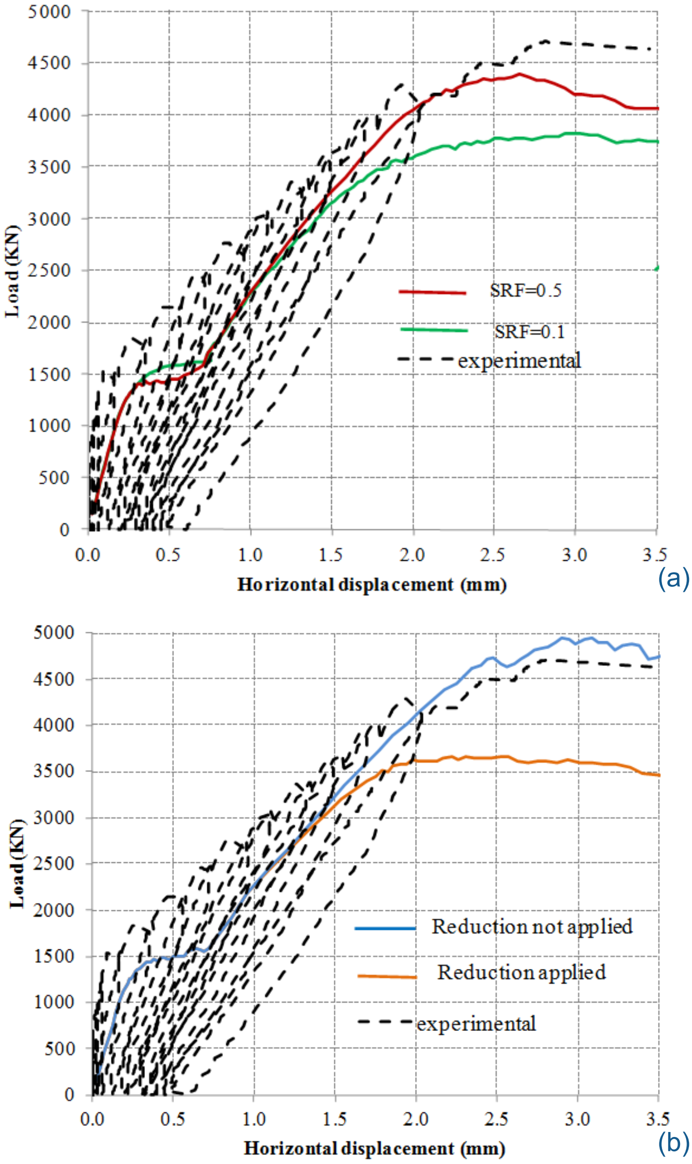

Figure 5. Load-displacement curves: (a) shear retention factor effect, (b) interaction model effect

Another parameter that can significantly influence the results obtained, especially in case of shear-compression failure, is the interaction model used: the software used doesn't put any low limit to the reduction of the compressive strength due to lateral cracking that can in this way theoretically reaches 100%. In Fig. 5(b) the interaction model effect is reported.

Because of computational time, both Fig. 5(a) and Fig. 5(b) refer to monotonic loading.

Conclusion

From the aforementioned observations it can be concluded that the general behavior of the squat wall is well predicted by the numerical simulations carried out with the finite element code DIANA 9.3. As observed in the experiments, the squat wall fails in shear due to crushing of concrete in the lower right part of the wall and under the loading plate without any reinforcement yielding.

The ultimate load value reached in the numerical simulations and the stiffness of the structure are strongly influenced by some parameters inputted in the analyses regarding the crack model adopted, such as the aggregate interlock effect, the tension stiffening effect and the interaction model. If these parameters are properly calibrated the ultimate load is well predicted by the numerical simulations.

References

[1] DIANA Release 9.3, Latest Update: Nov.27 12:02:30, 2008.

[2] www.concrack.org

[3] 2nd Workshop on " Control of Cracking in R.C. Structures", 20-22 June, Paris, France.

[4] Vecchio, F.J., Collins, M.P. (1993). *"Compression response of cracked reinforced concrete", J.Struct. Eng., 119, 3590-3610.*

NEW STAFF AT TNODIANA BV

In 2011 the TNO DIANA team has been strengthened by three new staff members:

Maziar Partovi has phD degree from Swansea University in Computational Mechanics and 7 years experience in international marketing and support of finite element software. TNO DIANA is pleased to have Maziar as sales and support engineer for DIANA on board.

Andreas Buykx and Xander Burgerhout have both a background as electrical engineers and 10 years' experience in development of scientific analysis & visualization software. Both Andreas and Xander have joined the TNO DIANA development team as senior developers and are working on graphical applications related to the DIANA software.

EVENTS

Courses

Throughout 2011 we have held a number of International training courses, both at our Headquarters in Delft and off-site. These courses have been open to the public and have attracted participants from all over the world.

Our standard courses consist of:

- A general introduction to DIANA
- Finite Element Analysis of (Reinforced) Concrete Structures
- Finite Element Analysis of Dams & Dikes
- Finite Element Geotechnical Analysis

Following the appreciative feedback of our students, we will be running these courses again in 2012, of course these will include updates where applicable. We will announce new dates on our website throughout 2012 at http://tnodiana.com.


RC Course, Delft, The Netherlands - May 11'


Geotechnical Course, Istanbul, Turkey - September 11'


RC Course, Delft, The Netherlands - October 11'


Dams Course, Delft, The Netherlands - Nov 11'

Online Training

In addition to our International training courses, we have recently introduced an online training programme. Again, these courses are open to the public and can be attended not only on your PC, but also on your tablet or smart-phone!

The courses are free of charge and are run both in the morning and evening to cater for our international contacts. By providing this service we hope to provide users a brief insight into the DIANA software and it's range of capabilities.

Each month we will be running both our "Introduction to DIANA" course and a specialist course "of the month", so keep an eye on the website for news about the programme.

We just released the dates for our Online Training courses in January and will soon add more dates

Keep an eye on the website for these!

Keep up to date...

With so much going on, it's easy to miss an event or a interesting piece of news. To make sure that you don't, sign up for our newsletter at http://tnodiana.com and click on the Newsletter Signup link.

We promise not to bombard you with rubbish on a daily basis, just an occassional message with news about new releases, courses and seminars and, of course, you can cancel your subscription at any time!

http//tnodiana.com

TNO DIANA BV
Delftechpark 19a
2628 XJ
Delft
The Netherlands

Tel: +31 (0) 88 34262 00
Fax: +31 (0) 88 34262 99

http://tnodiana.com

TNO DIANA
A TNO Company